UNIVERSITY OF CALIFORNIA, SAN DIEGO

Crack detection diagnostics using ultrasonic insonification

A thesis submitted in partial satisfaction of the
requirements for the degree
Master of Science

in

Structural Engineering with specialization in Structural Health Monitoring,
Prognosis and Validated Simulations

by

Gregory James Sylvester Jarmer

Committee in charge:

Michael Todd, Chair
Charles Farrar
William Hodgekiss

2009

The thesis of Gregory James Sylvester Jarmer is approved, and it is acceptable in quality and form for publication on microfilm and electronically:

_____

_____

_____

Chair

University of California, San Diego

2009

DEDICATION

To all the people who helped me get to where I am.

EPIGRAPH

It is time.
—J.J.J.

TABLE OF CONTENTS

LIST OF FIGURES

LIST OF TABLES

ACKNOWLEDGEMENTS

Chapter 3, in part, is a reprint of the material as it appears in *Smart Structures and Materials & Nondestructive Evaluation and Health Monitoring*, Gregory J. Jarmer, Michael D. Todd, 2009. The thesis author was the primary investigator and author of this paper.

Chapter 4, in part, is a reprint of the material as it appears in *Smart Structures and Materials & Nondestructive Evaluation and Health Monitoring*, Gregory J. Jarmer, Michael D. Todd, 2009. The thesis author was the primary investigator and author of this paper.

VITA

2006	B. S. in Mechanical Engineering, Oregon State University
2009	M. S. in Structural Engineering with specialization in Health Monitoring, Prognosis and Validated Simulations, University of California, San Diego

PUBLICATIONS

Gregory J. Jarmer and Michael D. Todd, "Crack Detection diagnostics using ultrasonic insonification and pattern recognition", *Smart Structures and Materials & Nondestructive Evaluation and Health Monitoring*, 2009.

ABSTRACT OF THE THESIS

Crack detection diagnostics using ultrasonic insonification

by

Gregory James Sylvester Jarmer
Master of Science in Structural Engineering with specialization in Structural Health Monitoring, Prognosis and Validated Simulations

University of California San Diego, 2009

Michael Todd, Chair

Sudden crack growth has the potential to cause catastrophic failure when a crack reaches a critical crack size. Early detection of crack formation minimizes this potential. This research focuses on the use of guided ultrasonic waves (GUWs) to detect crack formation. Experiments conducted on aluminum test specimens grew fatigue cracks through cyclic loading. Macro Fiber Composite (MFC) and piezoelectric disc transducers induced and received various GUWs ranging in frequency from 25 to 100 kHz. Features were extracted and correlated to crack length in the time domain, frequency domain and from autoregressive models of time series sensor data.

Chapter 1

Structural Health Monitoring

1.1 Introduction

Everyday, people throughout the world rely upon a wide range of engineering infrastructure, e.g. complex transportation networks such as automobiles bridges or aircraft, to perform all of life's necessities. This reliance is predicated upon these systems performing safely and consistently, as failure typically results in serious life safety or economic consequences. Many systems are used past their designed life expectancy, due to economic constraints [4, 5]. Using complex systems in spite of age and damage accumulation compounds economic and safety risks. In response to this, tools are being developed to detect the formation of damage in both new and aging infrastructure. Several disciplines are focused on damage detection in aerospace, civil, and mechanical systems, including Condition Monitoring, Non Destructive Evaluation (NDE) and Structural Health Monitoring (SHM) [6].

NDE consists of local off-line inspection to determine the presence of damage. Often the probable location and type of damage is know ahead of time, such as crack growth around a stress concentration. Structural Health Monitoring (SHM) is the process of implementing a damage detection strategy in near real time using periodic inspections of a system to determine the presence of damage. Inspection involves acquisition of the system's dynamic response, extraction of damage sensitive features from the response, and classification of the extracted features to determine health status. Condition monitoring is similar to SHM but applied explicitly to rotating machinery. SHM

was developed by expanding upon the theories of NDE and condition monitoring.

SHM improves upon NDE in two ways:

1. SHM is implemented in near real time with the system in operation or on-line. NDE requires off-line inspection which is undesirable for mission critical systems that are either in continual operation or must be available at any moment.

2. SHM often uses global inspection techniques implemented automatically by software, enabling the inspection of an entire system for damage. NDE generally uses local inspection techniques performed manually by a technician. Manually inspecting an entire system is often not physically or practically possible due to time and cost constraints.

This thesis focuses on detection of fatigue cracks in metallic structures using an SHM approach. In particular, feature extraction techniques using Guided Ultrasonic Waves (GUWs) are studied to determine the presence of crack formation. The thesis is organized into five chapters. Chapter 1 gives an overview of the SHM process and the steps for implementation. Chapter 2 covers background information about GUWs and gives a summary of published research and techniques to detect crack formation. Chapter 3 details experimental work performed to investigate the sensitivity of GUW at detecting fatigue crack formation. Chapter 4 covers results of detecting fatigue crack formation from time series analysis of received GUW waveforms. Chapter 5 gives a summary of results and issues that need to be addressed in future work.

What follows in this chapter is the motivation behind SHM and an overview of the SHM process.

1.2 SHM Motivation

As alluded above, the detection and diagnosis of damage is desirable in any system to improve safety, reduce costs and increase performance.

A recent example of catastrophic failure is the crash of Chalks Ocean Airways Grumman G-73T Turbo Mallard in 2005. Fatigue cracks in the right rear spar cap caused the crash, which claimed the life of all passengers and crew [1]. Figure 1.1 shows fatigue crack formation and propagation in the right rear spar cap, where smooth areas

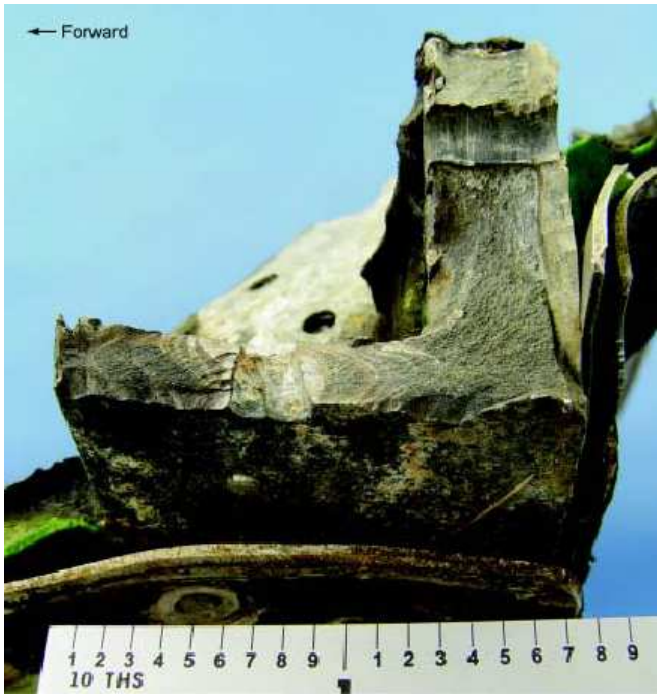

Figure 1.1: Fatigue crack initiation and growth in lower rear spar cap of right wing [1].

indicate gradual fatigue crack growth and rough areas rapid crack propagation [1]. The Federal Aviation Administration (FAA) stated that the root causes of the crash were (1) the failure of Chalks's Ocean Airways maintenance program to identify and properly repair fatigue cracks and (2) the failure of the FAA to identify problems in Chalk's Ocean Airways maintenance program [1].

The Aloha Airlines accident involving a Boeing 737 is another well known accident in which the upper skin of the fuselage became dislodged during flight, Figure 1.2. Improper bonding of a lap joint during manufacturing of the airplane allowed for premature corrosion and fatigue crack growth around rivet holes, which ultimately caused the failure of fuselage [2]. Here again the FAA stated the root cause of the problem as the failure of Aloha Airlines maintenance program to properly detect disbond and fatigue crack damage. Implementation of SHM systems that monitor for the formation of damage, such as fatigue cracks, have the potential to improve safety and reduce the chance of such accidents from occurring.

Prevention of catastrophic failure in civil systems is equally, if not more impor-

Figure 1.2: Damage of fuselage due to fatigue crack growth initiated by disbond of lap joint [2].

tant, since the potential for tremendous loss of life increases for failure of infrastructure that people occupy. In 2008, a residential natural gas pipeline ruptured resulting in an explosion killing one resident, completely destroying three homes and damaging 11 others, Figure 1.3 [3]. The pipeline ruptured due to fatigue crack formation initiated from damage caused by improper excavation of a nearby sewage line in 2003 [3]. The failure of other civil infrastructure such as bridges is a concern as well. It is estimated that over 40% of bridges in the United States are either structurally deficient or functionally obsolete [7]. The catastrophic failure in 2007 of the I-35W bridge in Minneapolis, MN highlights the need for SHM systems in civil infrastructure not only to improve safety, but performance as well. By measuring the current damage and operational load levels, the performance of the system may be optimized by calculating the maximum allowable operating conditions.

Another benefit of SHM is the reduction of costs associated with inspection and maintenance. The increasing number of aging aircraft in both civil and military sectors is a major problem due to the cost of inspection and maintenance, Figure 1.4. In 1999, 46% of US and European built civil aircraft in use were greater than 15 years old [5]. Ongoing midlife updates of military aircraft are increasing service life up to 50 years [8]. The implementation of an SHM system to monitor metallic aerospace components potentially reduces life cycle cost (LCC) by 50% [9].

The high cost for inspection and maintenance of civil infrastructure is similar to

Figure 1.3: Leaking gas line and resulting damage to resident's house [3].

that of aircraft. Maintenance costs for long span bridges can exceed $10,000,000 and for major repair $100,000,000 [12]. An SHM system that reduces maintenance cost is a great incentive to owners [12]. Currently many companies use time-based methods of maintenance where parts are replaced using a predetermined schedule, regardless of damaged status. Condition based maintenance saves the cost of unnecessary labor and replacement parts where only damaged parts are replaced. SHM allows the implementation of condition based methods through the early detection of damage [5, 6, 13].

The ultimate vision of the SHM field is to develop a system that continuously monitors a structure's health status. Real time data supports performance-level decision making, such as performance optimization or preventative maintenance. The reliability of the structure increases while cost of inspection and maintenance decreases. SHM systems need to be retrofitted to existing infrastructure and developed in conjunction with future systems where sensors and other monitoring devices are structurally integrated. This is important for future applications involving novel materials in which material characteristics and susceptible failure modes are relatively unknown.

(a) DC-9 aircraft [10] (b) F-16 aircraft [11]

Figure 1.4: Civil and military aircraft still in service: (a) DC-9 originally began production in 1965. (b) F-16 originally began production in 1974.

1.3 SHM Damage Paradigm

As stated in Section 1.1, Structural Health Monitoring (SHM) is the process of implementing a damage detection strategy in near real time using periodic inspections of a system over time to determine the presence of damage. Inspection involves acquisition of the systems dynamic response, extraction of damage sensitive features from the response, and then classification of the extracted features to determine health status. Features are extracted and classified through a statistical pattern recognition paradigm that uses the comparison between undamaged and damaged system states. To illustrate this process, view Figure 1.5 and answer the question, "Is this bridge damaged?" The answer is yes. The bridge is fractured which adversely affects its current and future performance. We arrived at this conclusion by comparing a mental picture of the damaged bridge to an undamaged bridge. This comparison is a pattern recognition process where differences between two system states identifies damage.

1.4 SHM Process

The SHM process is a combination of the following procedures [13]:

1. Operation evaluation
2. Data acquisition
3. Feature extraction

Figure 1.5: Example of statistical pattern recognition paradigm for a damaged bridge.

4. Classification

Figure 1.6 is a flow chart of the SHM process where each procedure is visually represented.

1.4.1 Operational Evaluation

The operational evaluation procedure defines high level aspects of implementing an SHM system. This includes justification for implementing a system such as an increase in safety, reduction in operating costs, or performance improvement. Additionally, a system is characterized by defining operational aspects and functionality. The procedure specifies damage type, location and other variables such as size and orientation. The operational evaluation clearly defines the problem aiding in the rest of the SHM process.

1.4.2 Data Acquisition

The data acquisition procedure determines a damage detection and implementation method for damage defined in the operational evaluation. For example, ultrasonic waves is one detection method for fatigue cracks. An implementation method would involve the use of transducers to induce ultrasonic waves in the structure, a data acquisition system to collect sent wave forms, and infrastructure for data transmission/processing.

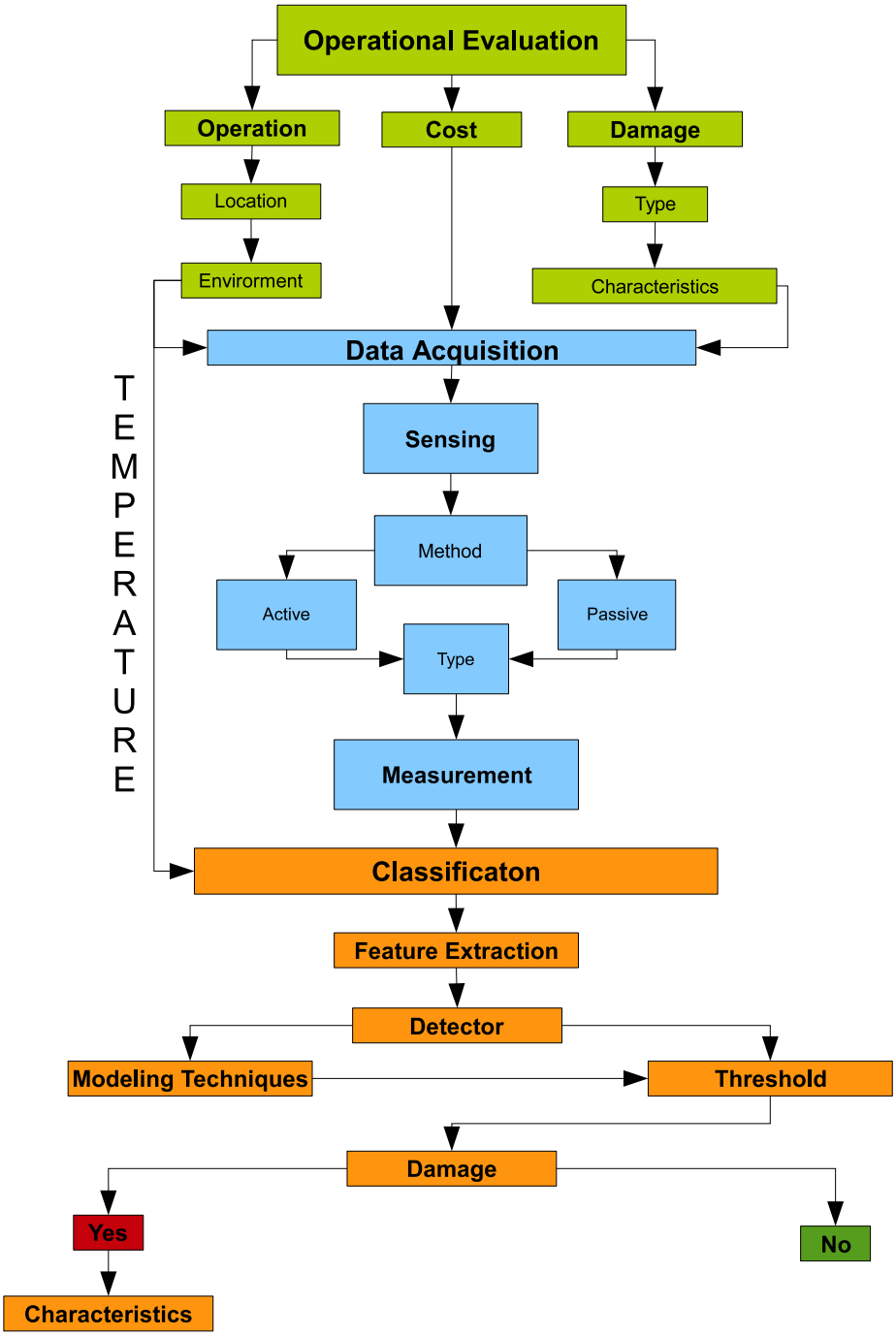

Figure 1.6: SHM Process

These aspects are system dependent and largely dictated by requirements defined in the operational evaluation.

1.4.3 Feature Extraction

The feature extraction process involves the extraction of damage sensitive features from sensor data collected during the data acquisition procedure to determine the presence of damage. The extraction of features is done through signal processing of sensor data, which includes the processes of data normalization, compression and fusion. Data normalization reduces sensitivity to environmental variability such as temperature fluctuations. The data compression process decreases the dimensionality of the acquired data. Data fusion involves combining data from multiple transducers to aide in feature identification.

1.4.4 Classification

The statistical modeling procedure aids in the proper classification of extracted features for various damage levels. There are generally two classes of statistical models used in the SHM process. The first class is supervised learning where a training set of known damage states is used to help classify extracted features. The second class is unsupervised learning where feature classification is based upon statistics of a given process [14].

1.5 Thesis Focus

The research for this thesis focuses on feature extraction and detection techniques in the classification section of Figure 1.6. These techniques use GUW time series data to detect the formation of fatigue cracks. An experiment is designed to induce fatigue cracks in a test specimen. GUWs are induced and measured at various damage levels (fatigue crack lengths). Features are extracted from the GUW time series data and correlated to fatigue crack. What follows in the next chapter is background information on elastic waves and a literature review of feature extraction and damage detection techniques using GUW's.

Chapter 2

Feature Extraction Techniques

2.1 Introduction

The use of elastic waves/stress waves for damage detection is one of the most popular methods in the fields of NDE and SHM. Ultrasonic waves are elastic waves with frequency greater than 20,000 kHz. Guided Ultrasonic Waves (GUWs) are ultrasonic elastic waves that utilize the waveguide properties of a structure to propagate. GUWs interact with a structure's geometry and internal defects resulting in scattering, attenuation, and mode conversion. Damage detection with GUWs takes advantage of this interaction to detect, locate, and possibly quantify defects or damage [15]. Damage-sensitive features are extracted from GUW time series data through signal processing techniques and correlated with damage that is to be detected. Signal processing techniques are broadly divided into four areas: time domain, frequency domain, time-frequency domain and modeling techniques.

What follows in this chapter is a brief background of elastic wave propagation, common sensing methodologies used with GUW's and a literature review of the above signal processing techniques applied to GUWs.

2.2 Waves Propagation Background

2.2.1 Elastic Waves

Elastic waves are stress waves that propagate in an elastic medium without transferring matter. Two types of elastic waves travel in extended isotropic solids; longitudinal and transverse waves [16]. Longitudinal waves, also known as compressional, dilatation pressure or P waves, are waves that propagate with particle motion in the direction of wave propagation. Transverse waves, also known as shear or S waves, are waves with particle motion perpendicular to the direction of wave propagation [17, 5]. Transverse waves are further classified as either Shear Horizontal (SH) or Vertical (SV) depending upon the associated direction of particle motion.

2.2.2 Guided Ultrasonic Waves

Elastic waves traveling and interacting with the boundary of the object are know as guided waves because the boundary makes the object act as a wave guide. Guided waves in an solid plate with free boundaries are known as Lamb waves. Lamb waves are the superposition of reflected longitudinal and transverse bulk wave modes [17]. This superposition results in the formation of two wave modes; Antisymmetric and Symmetric. Lamb waves are dispersive, meaning that the velocity of a traveling wave is dependent upon frequency. For a given frequency, multiple Lamb modes can exist.

GUWs for damage detection have two advantages over traditional ultrasonic techniques: (1) GUWs interrogate large areas of a structure for damage due to good propagation characteristics and (2) the high frequency (small wavelength) of GUWs allows for the potential of high sensitivity to small defects, where the size of the defect is commensurate with the GUW wavelength.

2.3 Sensing Methodologies

Ultrasonic waves are actuated and received/sensed in a structure with piezoelectric transducers using the reverse piezoelectric effect for actuation and the piezoelectric effect for receiving. Two sensing methodologies to induce and sense GUW's are:

Pulse-Echo

Pule Echo is when a single transducer acts as both an actuator and sensor. A single transducer first acts as an actuator by inducing a pulse and then as a sensor by listening/sensing for the echo/reflection from damage, Figure 2.1.

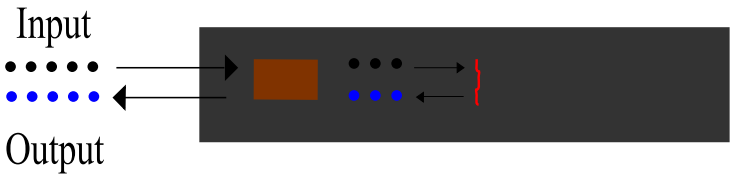

Figure 2.1: Pulse Echo Sensing Method

Pitch-Catch

Pitch-catch is when two separate transducers are used, one as an actuator and one as a sensor. The actuating transducer induces a GUW that travels through the structure to the sensing transducer, Figure 2.2.

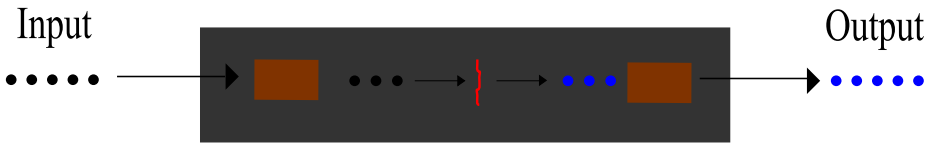

Figure 2.2: Pitch-Catch Sensing Method

Received waveforms that are sampled using an analog-to-digital converter are termed generally as time series data.

2.4 Feature Extraction Techniques

2.4.1 Introduction

Wave scattering occurs when an induced wave is perturbed by an inhomogeneity (damage) in the medium [18]. Scattering is a complex process that is dependent on the

damage geometry, induced wave properties, the elastic medium's material properties and other factors. The goal of the feature extraction process is to identify relationships between non scattered (not perturbed by damage) and scattered (perturbed by damage) waveforms, and to then use these relationships to characterize damage. Relationships are established by extracting damage sensitive features from time series sensor data through signal processing and then correlating with damage level. Signal processing techniques include time domain, frequency domain, time-frequency domain and modeling techniques [19]. Modeling techniques are further classified into physics-based and data-based techniques.

2.4.2 Signal Processing Techniques

2.4.2.1 Time Domain Analysis

Time domain analysis consists of extracting damage sensitive features from sensor waveforms in the time domain, where $x(t) = x[nT] = x[n]$ is a discrete time signal sampled every T seconds. All features extracted in the time domain are based upon the amplitude of the sensed waveform. Examples include:

1. Maximum Amplitude x_{max}
2. Minimum Amplitude x_{min}
3. Peak-to-peak Amplitude x_{pp}
4. Root Mean Square (RMS)
5. Mean $\bar{x}$
6. Standard deviation σ

The RMS of a signal defined as

$$x_{RMS} = \sqrt{\frac{1}{N}\sum_{i=1}^{N} x[i]^2} \tag{2.1}$$

is a measure of the amount of energy contained in a signal. Reference [20] detected fatigue crack formation in an aluminum plate using all the above features excluding x_{max} and $\bar{x}$.

Reference [21] conducted a similar fatigue crack experiment using a piezoelectric disc for actuation and a scanning laser vibrometer as a receiver in a pitch-catch configuration. Feature extraction analysis used the first two wave packages corresponding to the first wave arrival and reflection. The envelope of the received waveform was calculated using the Hilbert transform. The peak-to-peak amplitudes of the envelope functions for various damage levels normalized by the baseline undamaged condition were extracted as the damage sensitive feature. Reference [22] conducted a fatigue crack experiment using piezoelectric discs for actuation. The extracted feature is defined as

$$ExtractedFeature = \frac{R_{xy}}{\sqrt{R_{xx}R_{yy}}} \tag{2.2}$$

where R_{xy} is the cross correlation between a baseline condition and damaged state, and R_{xx}, R_{yy} are the associated autocorrelations.

The above features detect damage due to a change in the signal and are not able to provide any information regarding the location of damage. One method that allows for localization of damage is to use the subtraction of a baseline signal from a damaged signal. Subtraction results in a signal solely due to scattering allowing for the potential identification of reflections using time of flight and wave velocity. Reference [23] used this method to detect notch formation using tuned Lamb waves in pulse echo configuration.

2.4.2.2 Frequency Domain

Frequency domain analysis consists of transforming collected data from the time domain into the frequency domain using the Fourier transform. The Fourier transform is a linear transform, meaning that it satisfies the properties of superposition and scaling. GUWs are generally narrowband signals. Due to this, features extracted in the frequency domain based upon amplitude will correspond to features extracted in the time domain.

2.4.2.3 Time Frequency Domain

Lamb wave inspection is the most widely used damage detection technique based on GUWs [5]. The key problem in using Lamb waves for damage detection is the measurement of individual modes in the received multi-mode signal [24, 25]. Identifica-

tion of individual modes potentially allows for the identification of mode conversion and reflections due to defects. The Fourier transform in not appropriate to use in separating a non-stationary multi-modal signal because the Fourier transform is a global method that assumes stationarity. Time-Frequency domain techniques allow the analysis of non-stationary signals and are able to separate a multi-modal Lamb wave signal by taking advantage of the difference in group and phase velocities between modes. The short time Fourier transform ($STFT$) of a signal $x[n]$ given as

$$STFT = X[n, \lambda] = \sum_{m=-\infty}^{\infty} x[n+m]w[m]e^{-j\lambda m} \tag{2.3}$$

where $w[m]$ is a window sequence, is one such method. The $STFT$ converts a one dimensional sequence $x[n]$ into a two dimensional function of both time and frequency [26]. The modulus of the $STFT$, known as a spectrogram, corresponds to the time-frequency energy distribution of the signal. Reference [27] separated individual lamb modes using the spectrogram in a fatigue crack experiment and then estimated the amount of energy contained in the first arrival mode as a damage-sensitive metric. The ratio of energy for the first arrival mode between a baseline and damaged case was used as the extracted feature. The ability of the $STFT$ to resolve modes decreases when the time separation between modes decreases. Other Time-Frequency methods such as the Wigner-Ville distribution and matching pursuit method offer improved performance for separating modes [28, 25]. The discrete wavelet transform is another time-frequency method used to decompose a signal using a mother wavelet that is a function of time translation and dilation [5].

2.4.2.4 Modeling

2.4.2.4.1 Introduction

Predicting the interaction of Lamb modes with damage is a complex process often involving the use of a model. Feature extraction based upon modeling techniques is divided into two areas: 1) Physics-based and 2) Data-based models. Physics-based models use governing differential equations or finite element versions thereof to predict the interaction of GUWs with damage and boundaries. The predicted interactions are used as extracted features. Data-based models use a systems based approach where models

are established between input/output times series. Model coefficients or prediction error, the error of the model at predicting a known signal, are used as extracted features.

Physics-based models have the advantage that they predict the actual interaction of the GUW with damage. Knowing the scattering characteristics of a specific type of damage enables characterization of the damage such as size and orientation. Obtaining this amount of information however has the disadvantage of being computationally intensive. If the interactions of the propagating waves with boundary's are included in the model, the difficulty of the problem increases substantially. Furthermore, the exact scattering characteristics of highly specific defects (e.g., a corrosion spot, a weld crack, etc.) are highly complex, and waver interactions are very sensitive to these scattering characteristics. Predicting the interaction of a GUW with a defect and boundaries is not practical for real time SHM. Data-based models have the advantage that the complex interaction of the GUW with damage and boundaries is accounted for in the model. Disadvantages of a data driven approach are that a supervised learning method must be used in order to characterize damage.

2.4.2.4.2 Physics-Based

Numerous researchers modeled the scattering of Lamb waves with defects to aid in the interpretation of damage and the feature extraction process [24, 29, 30, 31]. Reference [24] studied the scattering of specific Lamb waves with defects using finite element models and verified the results experimentally. Surface breaking cracks where the depth, width and orientation of the cracks was varied to represent damage. Received Lamb waves were resolved in both space and time with a two dimensional Fourier transform. This allowed separation of the individual modes present in the multimodal received signal. The finite element and experimental results showed that the interaction of a single Lamb mode with a defect produces a mode conversion, i.e. a_0 mode to s_0 mode.

Reference [29] modeled the interaction of Lamb waves with a rectangular slot using the local interaction simulation approach (LISA) in conjunction with experimental work. A notch with varying width and depth represented damage. Sensor location relative to damage and boundaries determined the amplitude of the received Lamb waveform. Wave propagation distance and damage were shown to attenuate amplitude. However a

local increase in amplitude was observed due to reflections from damage and boundaries, showing that a feature extraction technique solely based upon wave attenuation is not a reliable damage indicator.

2.4.2.4.3 Data-Based

An alternative method for damage identification is through a data-based approach where the complicated interactions of lamb waves with damage and boundaries are considered as an observable output of a system. An example of a system with no damage is depicted in Figure 2.3 where $u(t)$ is a GUW input from a transducer and $y(t)$ is the received output of the GUW after traveling through the structure and interacting with boundaries.

An example of a system with damage is depicted in Figure 2.4, where damage is modeled as an external input $v(t)$ added to the system.

A systems approach transforms the damage identification problem to a system identification problem. A system is identified by forming a mathematical model using the input and output of the system. For a linear, casual, time invariant system, $y(t)$ is expressed mathematically as

$$y(t) = \sum_{k=1}^{\infty} g(k)u(t-k) + v(t) \tag{2.4}$$

where $g(k)$ is the systems impulse response [32]. Similarly $v(t)$ expressed in terms of an impulse response $h(k)$ and input $e(t)$, is expressed as

$$v(t) = \sum_{k=0}^{\infty} h(k)e(t-k). \tag{2.5}$$

Equations 2.4 and 2.5 when combined and expressed in terms of transfer functions is given as

$$y(t) = G(z)u(t) + H(z)e(t) \tag{2.6}$$

Figure 2.3: System with input and output

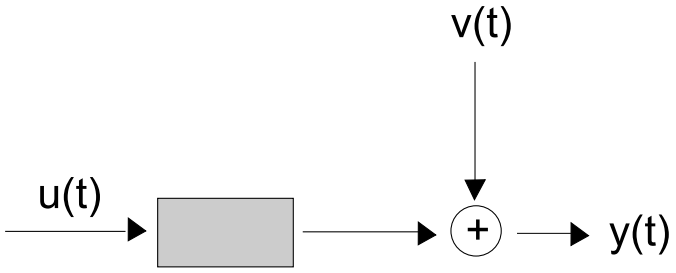

Figure 2.4: System with disturbance

where $G(z)$ and $H(z)$ are the z-transforms of $g(k)$ and $h(k)$ The system in Figure 2.4 is mathematically modeled using two approaches. The first approach creates a model incorporating physical insight through governing differential equations; a state space representation in continuous time is often used [32]. A second approach is a Black Box model that does not incorporate any physical insight. A model is formed using input output relations governed by a discrete linear difference equation. Reference [33] predicted the remaining life of a structure through a state space representation of fatigue crack growth and a GUW damage sensitive metric. Reference [34] detected the presence of damage in concrete columns with a black box model represented by an Autoregressive (AR) model of GUW's. The feature extracted for damage identification is the prediction error of the model for various damage levels.

Numerous other researchers have conducted research in this area [5, 17, 35, 36]. What follows in the next chapter is a detailed description of a fatigue experiment designed to allow for a thorough parametric study of applying GUW feature extraction techniques for fatigue crack detection.

Chapter 3

Experimental Design and Testing

3.1 Experimental Design

3.1.1 Test Specimen Design

Conducting an experiment involving crack formation poses two challenges; 1) control crack growth and 2) concurrently monitor the crack size. Growing a crack through fatigue solves both of these challenges by allowing controlled crack growth and providing the ability to pause testing for crack length measurement. With this in mind, the test specimen and fixture design were designed based upon the ASTM E 647 Eccentrically loaded Single Edge crack Tension specimen ESE(T).

Figure 3.1 shows an example of a test specimen and clevis used in this experiment. Aluminum 6061 T-6 was chosen for the specimen with dimensions of 14.5 (l) x 4 (w) x 0.25 (t) inches. A center notch was machined 0.25 inches perpendicular to the length staring at the center of the long edge, to act as a stress concentration for crack growth. Initial testing resulted in problems of random crack growth direction and shear lip formation. Side grooves were machined starting at the center notch and continuing through the width of specimen to prevent these problems. This improvement provided more accurate crack length measurements to better predict the corresponding load limits for fatigue growth.

The stress intensity factors for the ESE(T) specimen are determined using published empirical formulas [37]. The stress intensity factor for mode I loading is given

Figure 3.1: Clevis and test specimen

by,

$$k_I = F(a/b)\sigma\sqrt{\Pi a}, \tag{3.1}$$

where $F(a/b)$ is a geometry dependent constant, σ is the characteristic stress, and a is the characteristic crack dimension [38]. Fracture occurs when $k_I = k_{IC}$, where k_{IC} is the material dependent critical stress intensity factor. Using published values for k_{IC} of Al 6061 T-6, maximum load limits for fatigue cycling were estimated as a function of a, by solving for σ. Periodically throughout the experiment, the load was stepped down corresponding to crack length. To promote a high crack growth rate while buffering any crack length measurement error and preventing premature failure, 80% of k_{IC} was used to calculate the upper load limit. The lower load limit was calculated to keep the minimum to maximum force ratio constant throughout the experiment. This force ratio is given by,

$$R = P_{min}/P_{max}. \tag{3.2}$$

All fatigue cycles in this experiment used R $\approx$ 0.5.

3.1.2 Test Fixture Design

A clevis and pin assembly was designed to mount the test specimen based upon ASTM E 647 fixture recommendations. The clevis measured 4.8 x 2.4 x 1.5 inches with a pin diameter of 0.75 inches, Figure 3.2. Heat treated 4340 nickel chromium molybdenum was chosen as the clevis material for its high strength and resistance to galling and fatigue. The clevis was over designed to accommodate testing higher strength materials in the future. The clevis mounts to the thread rod on the Instron through a tapped hole.

3.1.3 Experimental Setup and Transducer Selection

Figure 3.3 shows test specimen and clevises assembled in a 110 kip MTS Instron. First, high strength thread rod is clamped in the wedge grips of the Instron, then the clevis assembly is threaded on. Finally, the test specimen is attached to the clevis through a pin connection. Figure 3.4 shows and a front and side view of the assembly.

Custom Matlab code utilizing the Data Acquisition Toolbox controlled the session. The data acquisition card, model PCI 6110 S by National Instruments (NI), sampled data at a rate of $4MS/s$ per channel with differential input. Nosie reduction

Figure 3.2: Clevis

proved to be one of the most challenging aspects of conducting this experiment. Custom signal conditioning on a shielded NI-SCB-68 connector block improved signal-to-noise ratio. Additionally, transducer connections using twisted shielded wire and a drain lead reduced sensor cross talk. The data acquisition improvements were essential due to a noisy testing environment.

MFC and piezoelectric discs were used as transducers to actuate and receive GUWs. MFC transducers consist of piezo ceramic rods encased in a flexible film and offer the advantages of directional actuation/sensing. The piezoelectric discs are omni directional and therefore have a better signal-to-noise ratio when compared to the uni-directional MFC transducers. The piezoelectric discs pick up the reflected waves from many directions resulting in a stronger signal.

A total of four MFC transducers were used during the experiment; two MFC transducers were bonded on each side (front and back) of the specimen so that sent signals would propagate through the fatigue crack growth area. The remaining two MFCs were bonded at the same coordinates, but on the back side. Figure 3.4 shows two of the MFCs bonded to the front side of the specimen. A total of four piezoelectric discs were also used. The discs were placed symmetrically around the fatigue crack area on only the front side of the specimen, see Figure 3.4. An aerospace grade epoxy, Loctite Hysol E-120HP, was used to bond the MFC transducers to the test sample. Additionally,

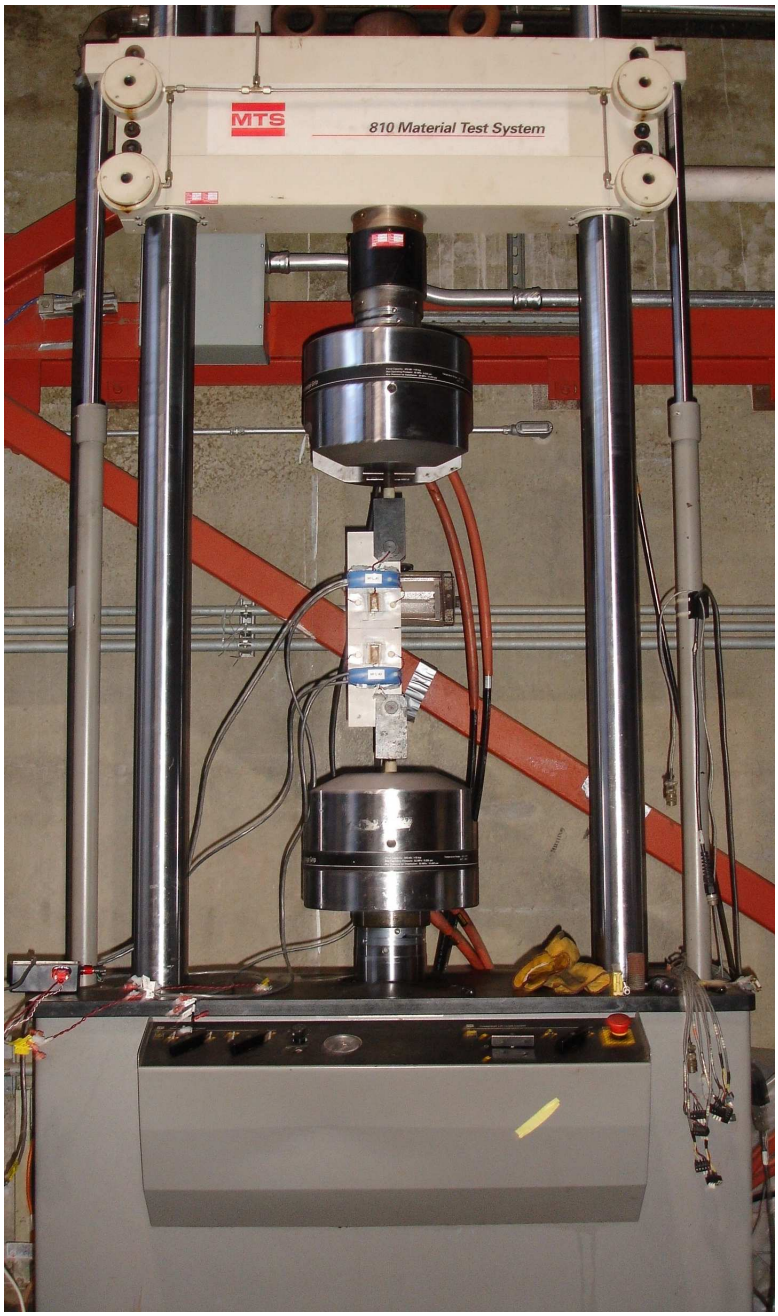

Figure 3.3: MTS tester with test specimen

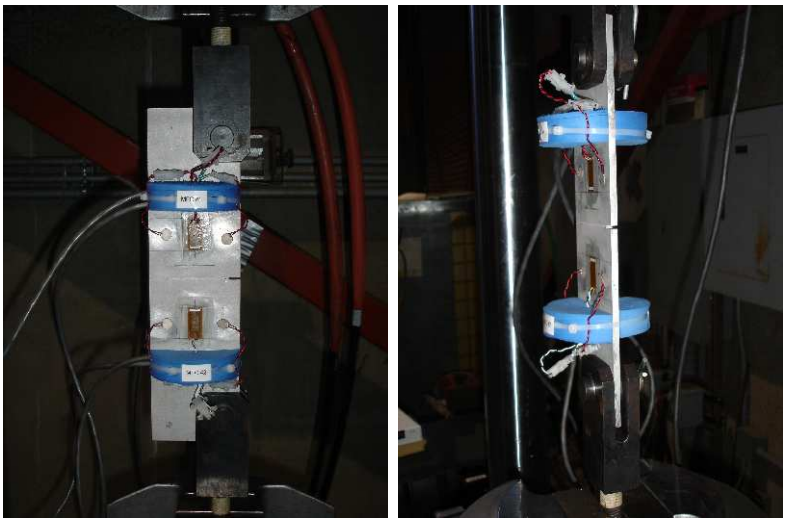

(a) Front View (b) Side View

Figure 3.4: Close up of assembled experimental setup

each MFC transducer cured under vacuum to assure proper bonding. Bonding of the piezoelectric discs is a simpler process because no vacuum bagging is required. In order to securely attach the wire connections to the transducers during fatigue testing and prevent disbond of the solder connections, blue circular strain reliefs were fabricated, see Figure 3.4. Dynamic testing environments require excellent strain relief.

3.2 Testing

3.2.1 Test Signals

The experiment used six test signals consisting of a Hanning windowed modulated sine burst and a chaotically modulated sine burst, each at frequencies of 25, 50, and 100 kHz. Chaotically-modulated signals are chosen due to a greater phase space diversity/density, which may allow for better sensitivity to damage using state-space based models. Table 3.1 is the test matrix used for the experiment. Figure 3.5 shows a received waveform where the actuation signal was a 25 kHz sine wave. Test signal frequencies were chosen based upon whether the shape for the first arrival of the received waveform matches with the shape of the sent waveform. Selection of the same shape

Table 3.1: Test matrix of actuation signals and transducers

		Modulated Sine (kHz)		
		25	**50**	**100**
Transducer	**MFC**	X	X	
	Piezo Disc	X		X

		Modulated Chaotic Sine (kHz)		
		25	**50**	**100**
Transducer	**MFC**	X	X	
	Piezo Disc	X		X

corresponds to selecting a frequency region that is relatively insignificant to dispersion (i.e., phase velocity is constant with frequency). The actuated signals have bandwidth due to modulation with the Hanning window. If signals are sent in a frequency range where dispersion is not constant, the received waveform will be distorted due to varying speeds of the frequency components in the wave packet.

3.2.2 Data Collection

The first step in the data collection process consisted of acquiring a baseline state of the test specimen with no damage. A test run then consisted of the following steps:

1. Fatigue the specimen using the calculated load limits previously discussed in Section 3.1.1.

2. Measure and record the fatigue crack length using a digital microscope.

3. The test signals outlined in Table 3.1 were sent and data collected at increments of approximately 0.075" of crack growth. Signals were sent with the specimen under zero tensile stress while mounted in the Instron.

Steps 1-3 describe a single test run. A total of 18 test runs were performed, corresponding to a final fatigue crack length of 1.4 inches. The numbering scheme for

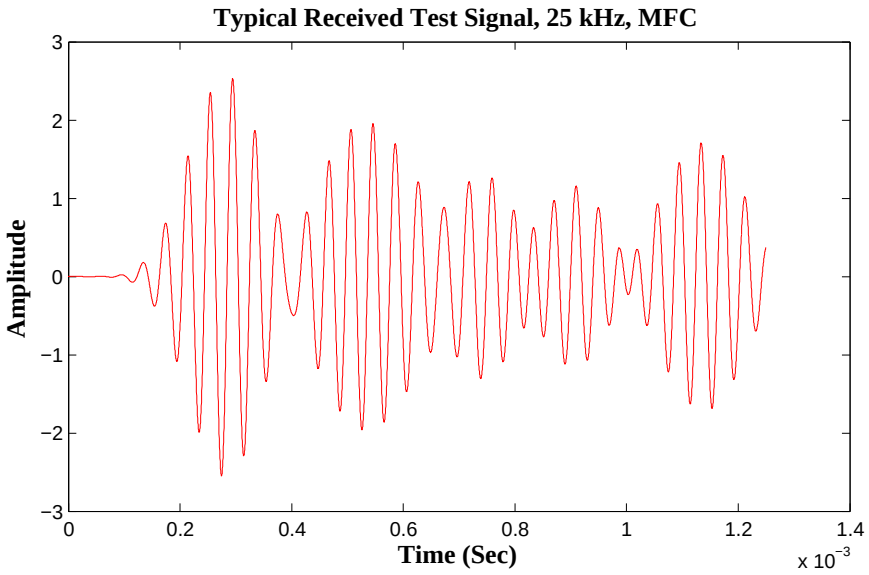

Figure 3.5: Typical Received Test Signal, 25 kHz, MFC

the MFC patch transducers is shown in Figure 3.6 where sensors 2 and 3 are orientated and positioned identical to sensor 1 and the actuating sensor but on back side of the test specimen. The numbering scheme for the piezoelectric discs transducers is shown in 3.7 where the transducers are numbered in the clockwise direction starting after the actuating sensor. Note that all of the piezoelectric disc transducers are on the one side of the test specimen, while the MFC patches are on both sides.

Chapter 3, in part, is a reprint of the material as it appears in *Smart Structures and Materials & Nondestructive Evaluation and Health Monitoring*, Gregory J. Jarmer, Michael D. Todd, 2009. The thesis author was the primary investigator and author of this paper.

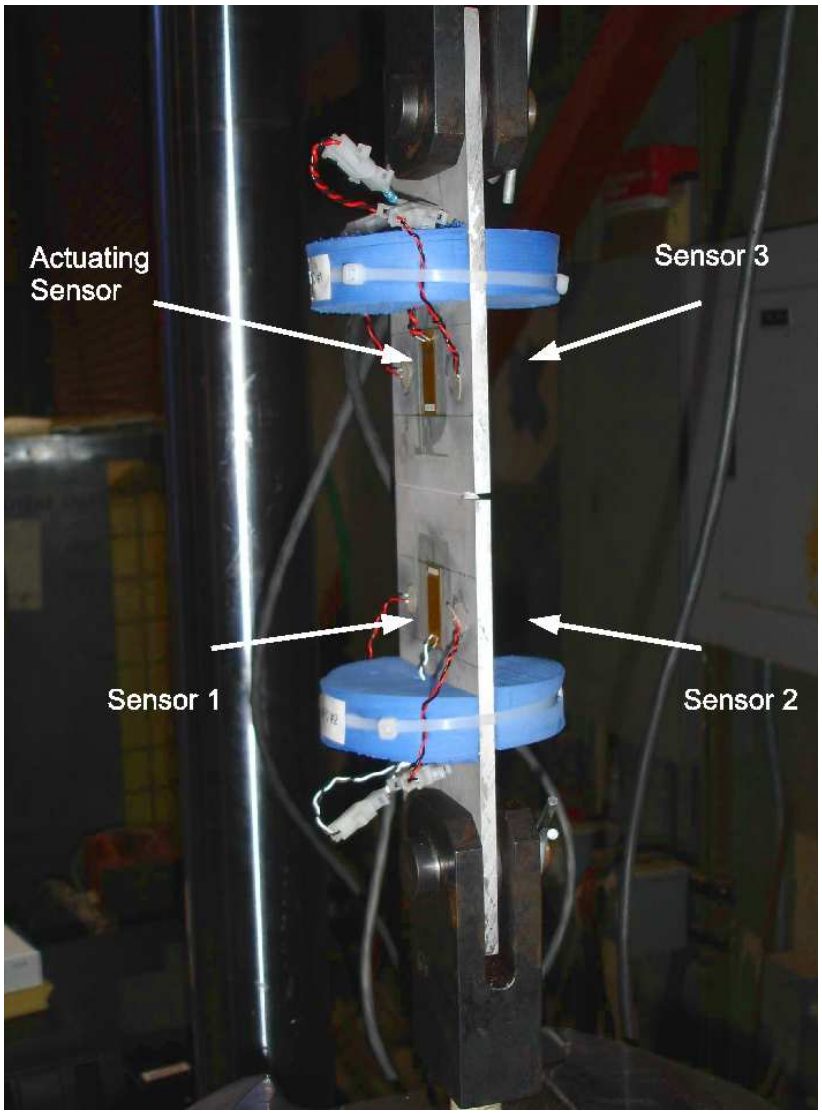

Figure 3.6: Side view of test specimens with MFC transducers labeled

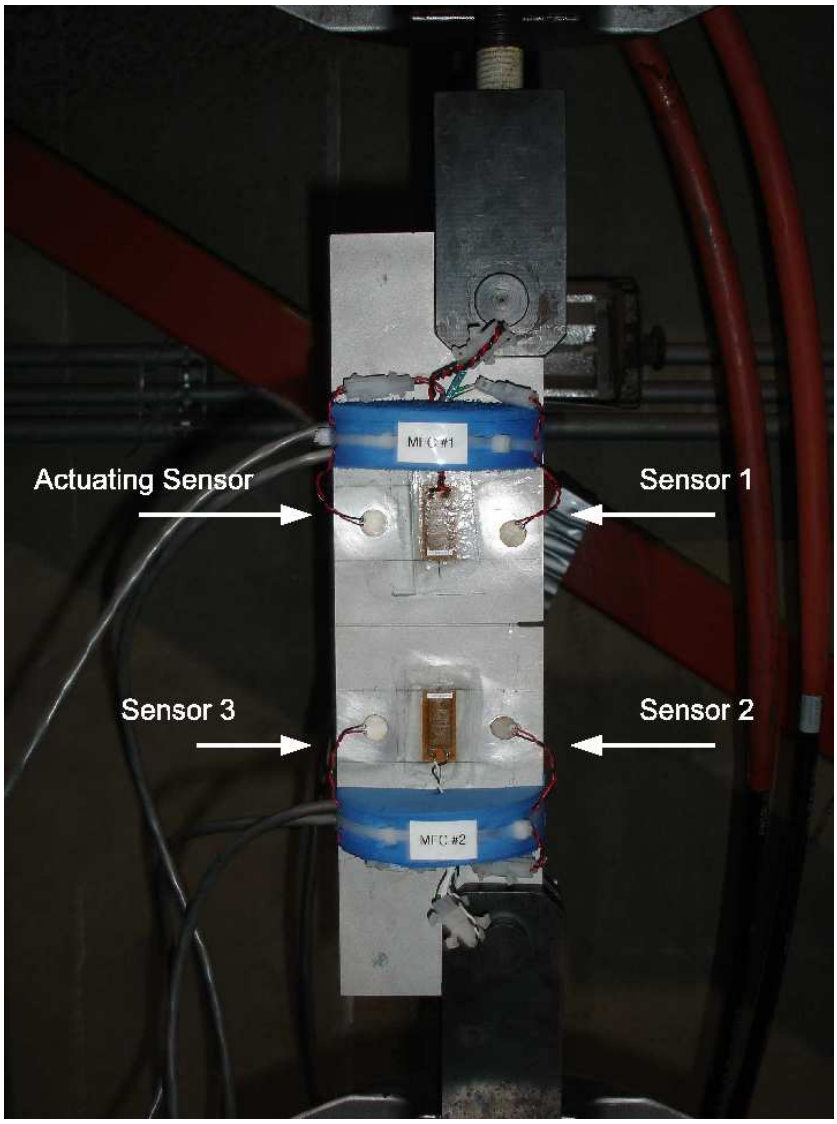

Figure 3.7: Front view of test specimens with piezoelectric transducers labeled

Chapter 4

Signal Processing Results

4.1 Introduction

The goal of this research is to detect crack formation with GUWs through the comparison of crack sensitive features. Figure 4.1 illustrates this process. An input signal is applied to an actuating transducer inducing a GUW. The GUW travels through the test specimen interacting with boundaries and any damage present along the propagation path. Upon arrival at the receiving transducer, the GUW is converted to an output signal (time series). A feature is extracted from the time series and correlated to crack growth. Feature extraction is accomplished through time domain, frequency domain, and modeling techniques. Results from each technique are presented in this chapter.

Time series data (single trial run) is composed of the time average of 50 indi-

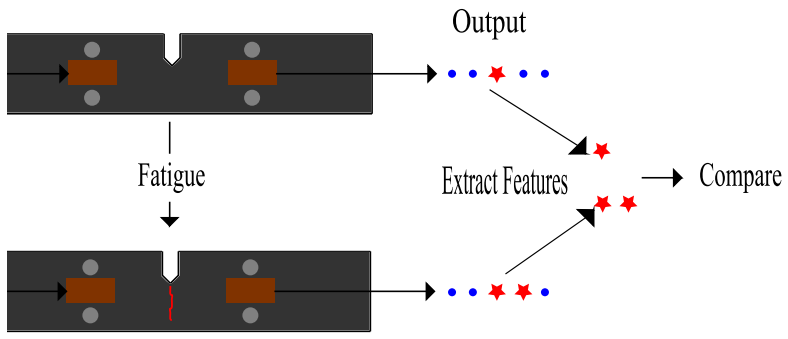

Figure 4.1: Damage detection through feature comparison

vidual sample runs. Sample runs are received waveforms for a given damage level. All time series data is preprocessed and normalized by a baseline, no damage present, time series before analysis. Normalization consists of subtracting the mean and dividing by the standard deviation of the baseline time series, Equation 4.1.

$$x[n]_{Normalized} = \frac{x[n]_{Damaged} - mean(x[n]_{Baseline})}{std(x[n]_{Baseline})} \tag{4.1}$$

Additionally all time series are convolved with respective input signal to remove any DC offset and high frequency noise. This is equivalent to bandpass filtering the signal since the input signal is narrowband. Analysis is performed on time series of two lengths. The first length includes only the first arrival of the received waveform, approximately 2000 points. The second length includes the entire length of the received waveform, 40,000 points. This separation into two lengths is due to physical intuition about how the GUW interacts with the fatigue crack (damage). The assumption is made that for the first arrival waveform, an increase in crack size (increase in damage) causes a decrease in the amount of energy transmitted (increase in path impedance) to the receiving sensors. The receiving sensors are sensors 1 and 2 for the MFC transducers, and sensors 3 and 4 for the Piezo disc transducers. See Figures 3.6 and 3.7 for sensor positions.

To simplify the presentation of results, plots are only shown for the first arrival waveform of the MFC transducer with actuation signal of 25 kHz sine wave. Results for other data lengths, actuation signals and transducers are given in tables 4.1 to 4.4.

4.2 Time Domain Analysis

Time domain analysis consists of extracting damage sensitive features from sensor waveforms in the time domain, where $x(t) = x[nT] = x[n]$ is a discrete time signal sampled every T seconds. Figure 4.2 is a plot of time series data and associated signal envelope for MFC sensors 1, 2, and 3 with a signal excitation frequency of 25 kHz. The signal envelope is obtained by taking the absolute value of the signal's Hilbert transform. Comparing the amplitude of the received waveforms shows how the amplitude varies in both time and position (sensor location). Variation is due to the complex interaction of the waveform with the geometry and/or induced damage of the test specimen resulting in a random nonstationary signal. This is shown more clearly in Figure 4.3, which is a

plot of the signal envelope for a baseline condition (no damage), first damage condition (crack length = 0.1 in) and the difference between the two (baseline - damage condition).

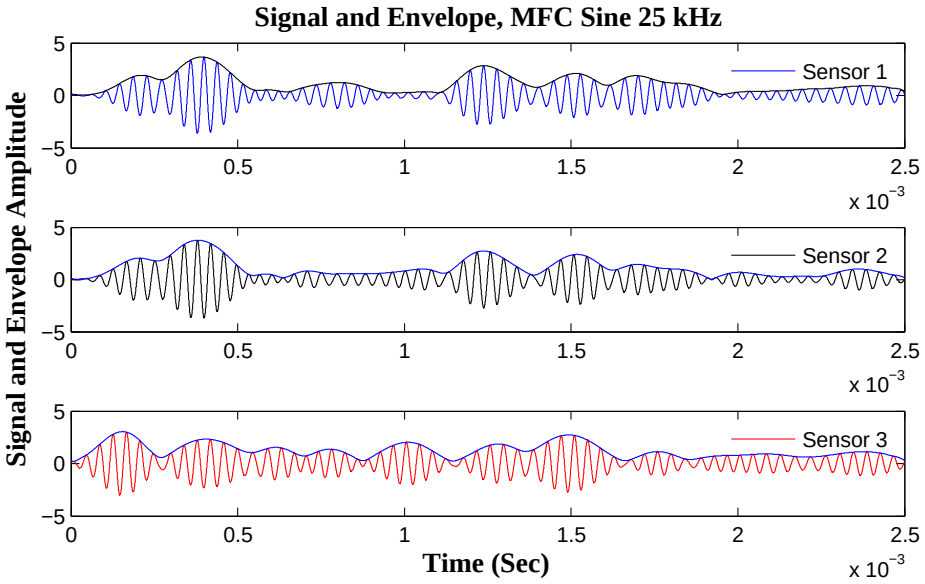

Figure 4.2: Signal and envelope of 25 kHz Sine: MFC transducer

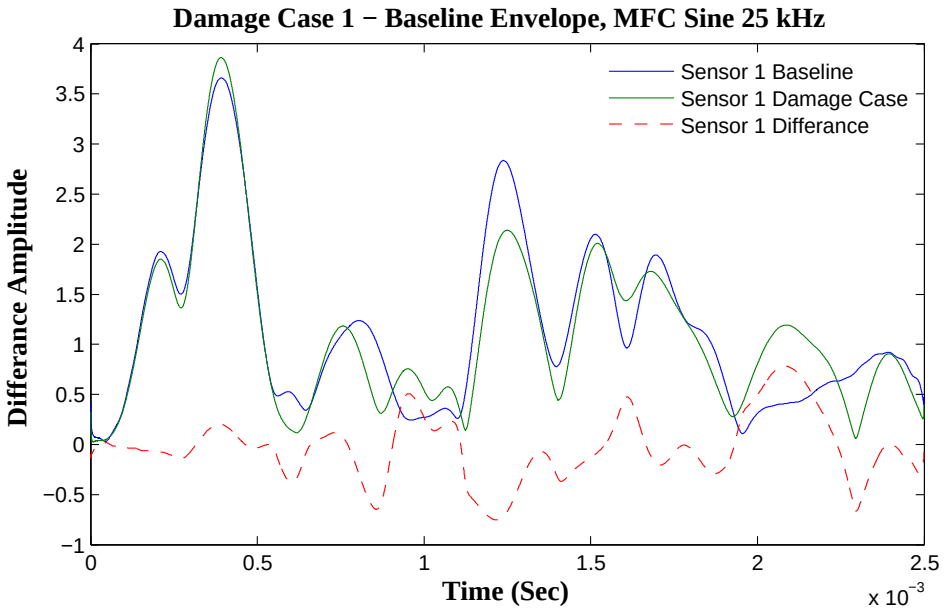

Figure 4.3: Baseline envelope minus damaged envelope of 25 kHz sine: MFC transducer

4.2.1 Max, Min, Peak-to-Peak and RMS Amplitude

In this section maximum, minimum, peak-to-peak amplitude and root mean square are studied as extracted features. Figure 4.4 is a plot of the maximum amplitude of the first arrival waveform verse crack length. Here sensors 1 and 2 show a decreasing trend in amplitude (negative slope) with increasing crack length. In contrast the amplitude of Sensor 3 does not show a strong correlation with increasing crack size. To aid in a general comparison of the sensor trends, a linear least squares line is fitted to the data. The slope value (m), is given next to the sensor name in the legend. Comparing the slope values of Figure 4.4 confirms visual intuition that sensors 1 and 2 are the most correlated with crack length and sensor 3 the least. A decrease is expected because sensors 1 and 2 are in the through transmission path of the crack while sensor 3 is not. Figure 4.5 is a plot of the normalized maximum amplitude with error bars of $\pm$ one standard deviation. The error bars are estimated by determining the variation of extracted features from individual sample runs. Due to the repeatability of sample runs, error bars are excluded from future plots.

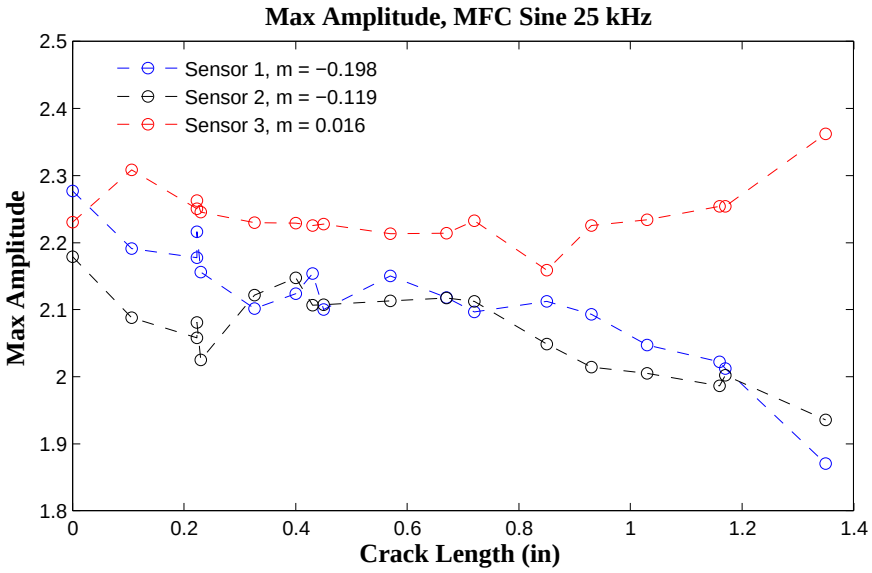

Figure 4.4: Maximum amplitude of 25 kHz sine: MFC transducer first arrival

Figures 4.6, 4.7 and 4.8 are plots of the minimum received, the peak-to-peak and the RMS amplitude. Here trends similar to the peak amplitude are obtained. The

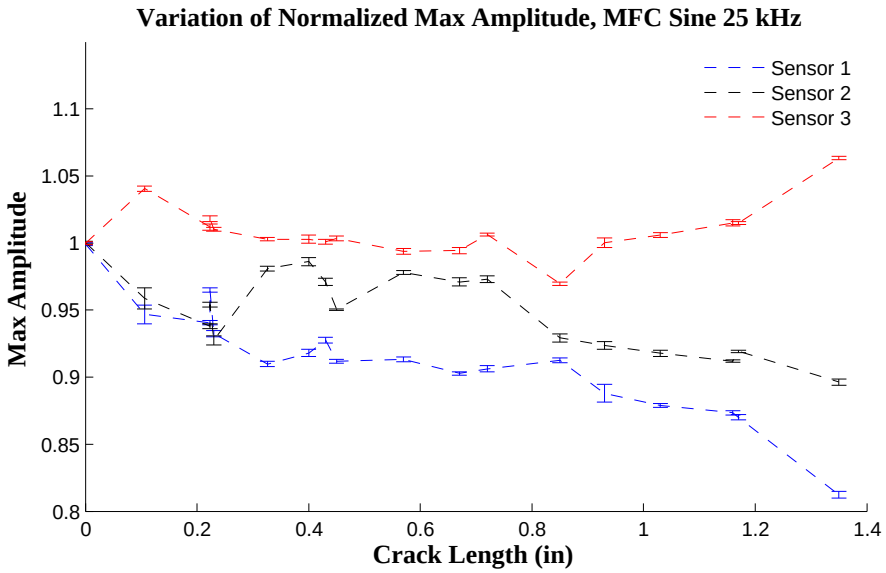

Figure 4.5: Maximum amplitude of 25 kHz sine: MFC transducer first arrival

magnitude of sensors 1 and 2 decrease while sensor 3 remains relatively constant. The RMS leads to a physical interpretation as the amount of energy in the received signal because it is a summation of amplitude squared terms. A decrease in RMS is a decrease in the amount of energy transmitted through the crack. A decrease in amplitude matches with the idea that an increase in crack length corresponds to an increase in path impedance, decreasing the amount of energy in the first arrival waveform.

Viewing Figures 4.4 through 4.8 there is a constant relationship where sensors 1 and 2 decrease in magnitude while sensor 3 stays relatively constant. These relationships hint at the idea of being able to combine the sensor pairs in various combinations to increase the correlation between signal amplitude and crack length. One possible feature is the pointwise product of the extracted feature for each sensor normalized by the number of sensors, given as

$$x_C^{Feature} = \prod_{i=1}^{n} \frac{Sensor_i}{n}. \tag{4.2}$$

Figure 4.9 is a plot of X_C^{PP} for the extracted feature of peak-to-peak amplitude. Here the correlation with crack length is increased compared to individual sensor peak-to-peak amplitude features, Figure 4.7.

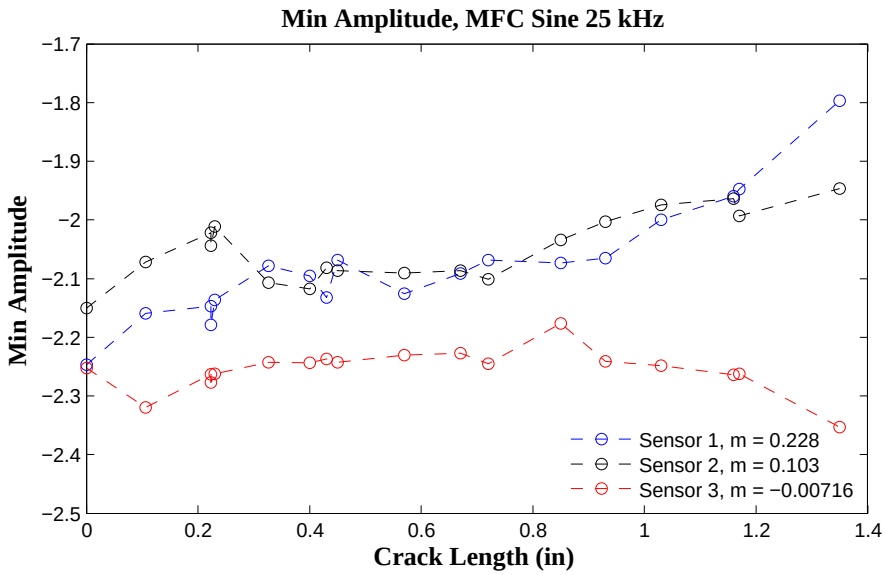

Figure 4.6: Minimum amplitude of 25 kHz sine: MFC transducer

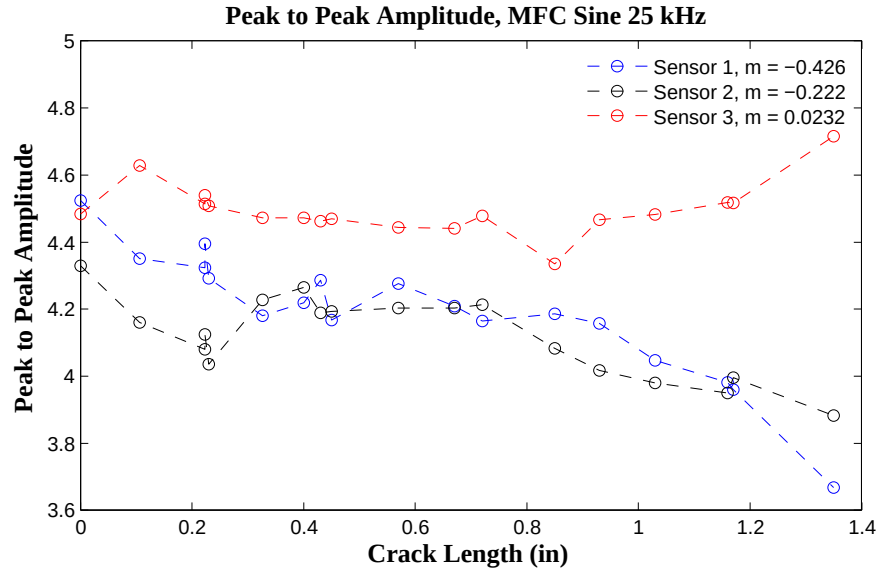

Figure 4.7: Peak to Peak amplitude of 25 kHz Sine: MFC transducer

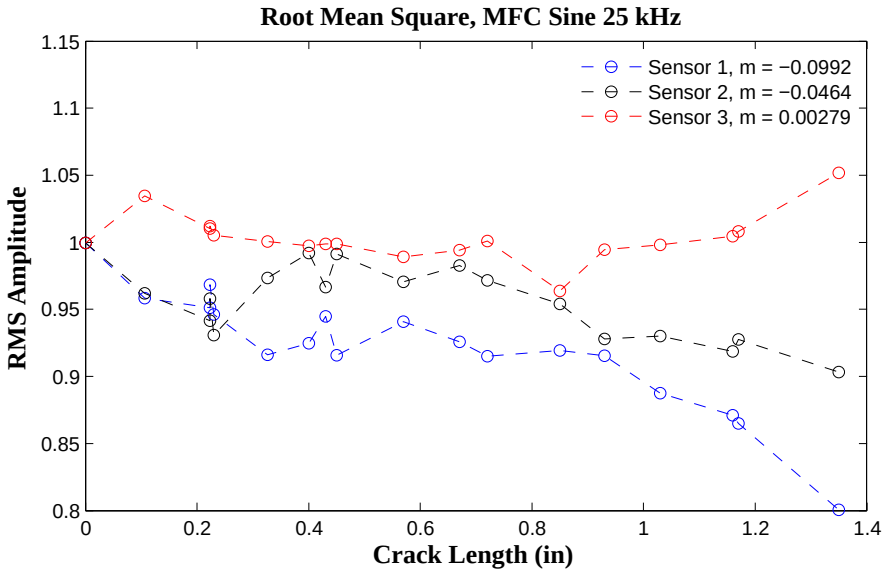

Figure 4.8: Root mean square (RMS) amplitude of 25 kHz Sine: MFC transducer

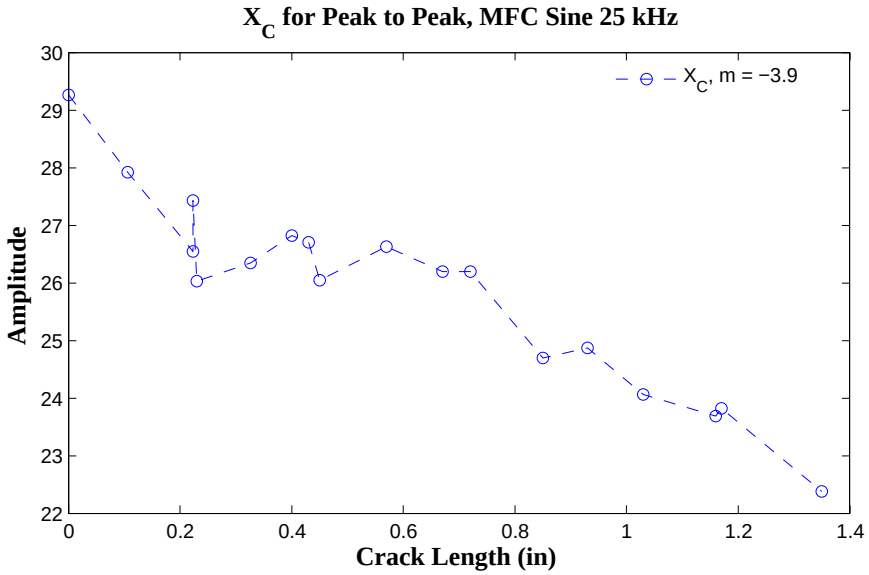

Figure 4.9: Combined extracted feature for Peak-to-Peak amplitude 25 kHz Sine: MFC transducer

4.2.2 Mean, Standard Deviation, Standard Deviation of Baseline Subtraction and Cross-Correlation Max

In this section the mean, the standard deviation ,the standard deviation of baseline subtraction and the max of cross-correlation are studied as extracted features. Figure 4.10 is a plot of the mean of the received signals, which shows no correlation to damage for any sensor.

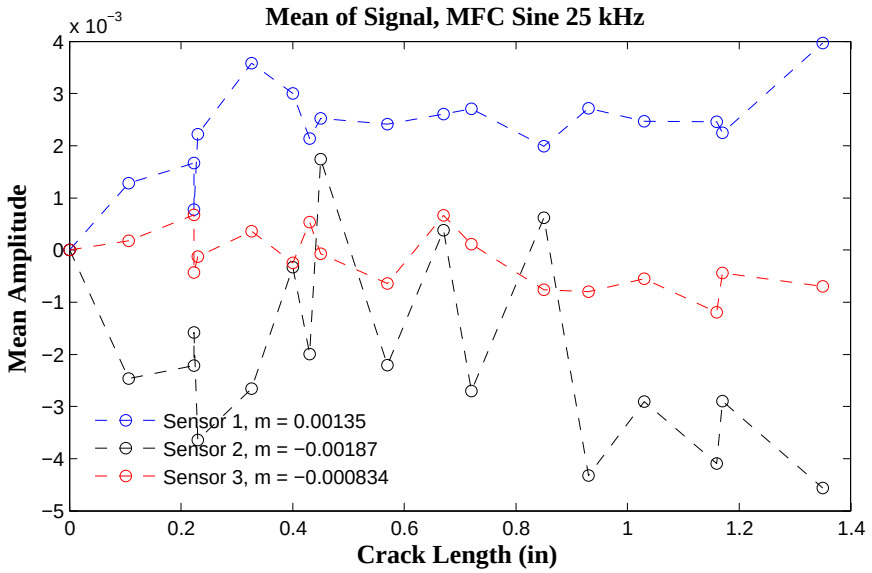

Figure 4.10: Mean of received signals. 25 kHz Sine: MFC transducer

The standard deviation of baseline subtraction, Figure 4.11, is formed by subtraction of the baseline envelope from the damaged signal envelope. See Figure 4.3 for example of baseline subtraction. Sensors 1 and 2 show an increase in magnitude with increasing crack length while sensor 3 remains relatively constant except for an increase at crack length of 1.3 inches. The cross-correlation max follows similar trends to that of the max amplitude where sensors 1 and 2 decrease while sensor 3 remain relatively constant, Figure 4.12.

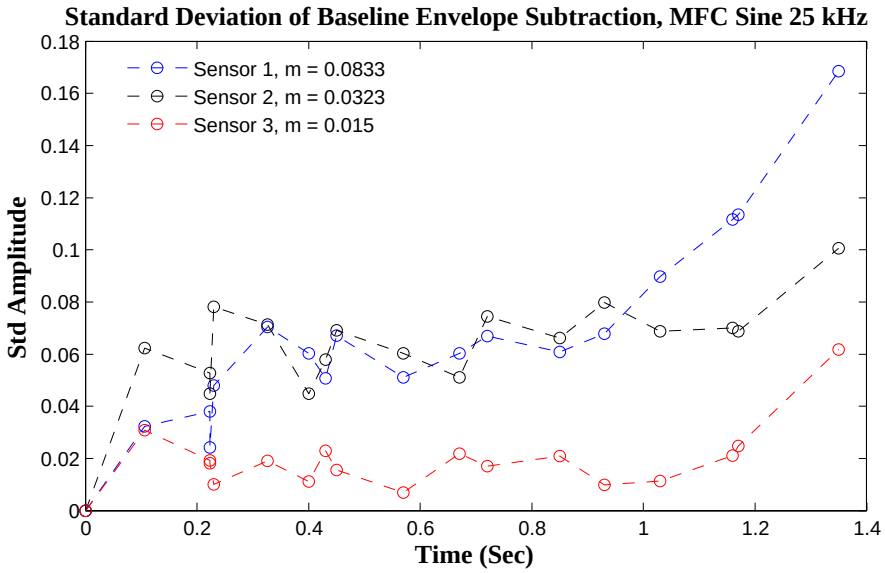

Figure 4.11: Standard Deviation of Baseline Envelope Subtraction. 25 kHz Sine: MFC transducer

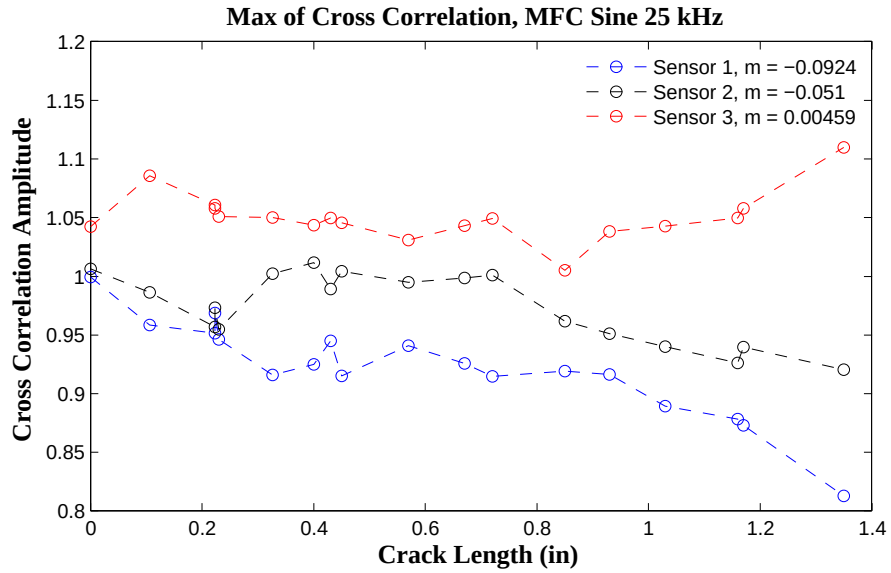

Figure 4.12: Max of Cross-Correlation. 25 kHz Sine: MFC transducer

4.2.3 Summary of Time Domain Analysis

Results for all actuation signals, transducers, and signal lengths are given in Tables 4.1 to 4.4. The labeling (1,2,3) corresponds to sensor 1, sensor 2 and sensor 3. The term ": 2^{nd}" means that the extracted feature is only able to detect change in the second half of the signal for crack lengths greater than 0.4 inches.

Table 4.1 lists results for analysis based upon the entire waveform length for the MFC transducers. Under these conditions, the best extracted feature is the standard deviation of the baseline subtraction (Std Diff). Overall the chaotically modulated waveforms perform better than the sinusoidal waveforms. All extracted features except for standard deviation and max of cross-correlation are only able to detect a change due to crack formation greater than 0.4 inches.

Table 4.1: MFC Transducer Results: Entire Signal Length

	Modulated Signal (kHz)			
	Sine 25	**Sine 50**	**Chaotic 25**	**Chaotic 50**
Max Amp	-	-	1,2:2^{nd}	2,3:2^{nd}
Min Amp	-	-	1,2:2^{nd}	2,3:2^{nd}
Peak-to-Peak	-	-	1,2:2^{nd}	2,3:2^{nd}
RMS	-	1,3:2^{nd}	1,2,3:2^{nd}	1,2:2^{nd}
Mean	-	-	-	-
Std	-	1,3:2^{nd}	1,2,3:2^{nd}	1
Std Diff	1,2,3:2^{nd}	1,2,3:2^{nd}	1,2,3:2^{nd}	1 2,3:2^{nd}
Max Cross Corr	1,2,3:2^{nd}	1	1,2,3:2^{nd}	1

Analysis based upon the first arrival for the MFC transducers is tabulated in Table 4.2. All extracted features have similar performance except for the mean. Additionally, the sinusoidal waveforms perform better than the chaotically modulated waveforms. This is in contrast to analysis based upon the entire waveform.

Table 4.2: MFC Transducer Results: First Arrival

	Modulated Signal (kHz)			
	Sine 25	**Sine 50**	**Chaotic 25**	**Chaotic 50**
Max Amp	1,2	1,2	1,2	2
Min Amp	1,2	1,2	1,2	2
Peak-to-Peak	1,2	1,2	1,2	2
RMS	1,2	1,2	1,2	1,2
Mean	-	1	-	1
Std	1,2	1,2	1,2	1,2
Std Diff	1,2	1,2,3	1,2	-
Max Cross Corr	1,2	1,2	1,2	1,2

Of the three sensors, sensors 1 and 2 perform best because sensors 1 and 2 are positioned down stream of the damage allowing the analysis of a waveform that is transmitted through the fatigue crack. In contrast sensor 3 is only able to detect damage due to reflections from crack formation, which explains it's poor performance.

Results for the piezoelectric disk are tabulated in Tables 4.3 and 4.4. Results are only listed for sensor 3 due to sensors 1 and 2 becoming disbonded during testing. For the entire signal length, the 100 kHz sine is overall the best performing signal. The cross-correlation max is best extracted feature. For the first arrival, the 25 kHz sine is the best performing signal with nearly equal performance for all extracted features.

Table 4.3: Piezo Transducer Results: Entire Signal Length

	Modulated Signal (kHz)			
	Sine 25	**Sine 100**	**Chaotic 25**	**Chaotic 100**
Max Amp	-	$3{:}2^{nd}$	-	-
Min Amp	-	$3{:}2^{nd}$	-	-
Peak-to-Peak	-	$3{:}2^{nd}$	-	-
RMS	-	$3{:}2^{nd}$	-	-
Mean	-	$3{:}2^{nd}$	-	-
Std	-	$3{:}2^{nd}$	-	-
Std Diff	-	-	-	3
Max Cross Corr	3	$3{:}2^{nd}$	3	3

Table 4.4: Piezo Transducer Results: First Arrival

	Modulated Signal (kHz)			
	Sine 25	**Sine 100**	**Chaotic 25**	**Chaotic 100**
Max Amp	3	$3{:}2^{nd}$	-	$3{:}2^{nd}$
Min Amp	3	$3{:}2^{nd}$	-	$3{:}2^{nd}$
Peak-to-Peak	3	$3{:}2^{nd}$	-	$3{:}2^{nd}$
RMS	3	$3{:}2^{nd}$	-	$3{:}2^{nd}$
Mean	-	-	-	$3{:}2^{nd}$
Std	3	$3{:}2^{nd}$	-	$3{:}2^{nd}$
Std Diff	3	$3{:}2^{nd}$	-	3
Max Cross Corr	$3{:}2^{nd}$	$3{:}2^{nd}$	-	$3{:}2^{nd}$

4.3 Frequency Domain Analysis

Frequency domain analysis consists of transforming collected data from the time domain into the frequency. The transformation of discrete time data is done through the discrete Fourier transform (DFT), which is computed using efficient Fast Fourier transform (FFT) algorithms. The DFT is a linear transformation meaning that it satisfies the properties of superposition and scaling.

Since the collected time series data is narrow band, extracted features in the frequency domain based upon amplitude will be similar to extracted features based upon amplitude in the time domain. To illustrate this, Figure 4.13 is a plot of the DFT of the first arrival for the 25 kHz sine waveform at various damage levels. The peak values of the DFT decrease with damage level/crack growth. A decrease is expected since the peak amplitude in the time domain shows the same relationship. Figure 4.14 illustrates the decrease more clearly by plotting the peak values of the DFT against crack length. Comparing Figures 4.4 and 4.14 for sensor 1, shows that they are nearly identical in shape.

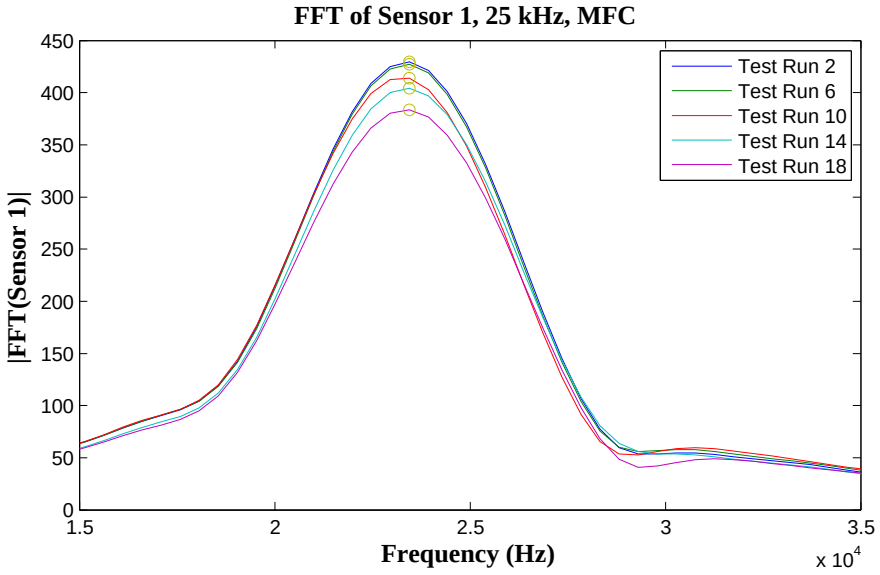

Figure 4.13: FFT of sensor 1, 25 kHz, MFC

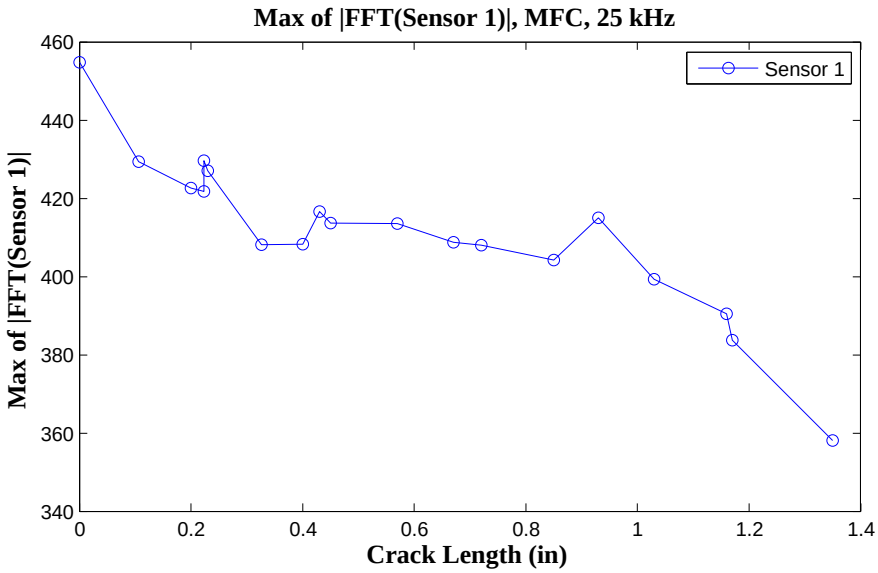

Figure 4.14: Max of FFT of sensor 1, 25 kHz MFC

4.4 Modeling Analysis

Section 2.4.2 detailed the idea of identifying damage using a system identification approach. A model is formed using input-output relations governed by a discrete linear difference equation, and then correlated to damage. Correlation is done through model parameters or prediction error. An example of a system model for feature extraction is the autoregressive (AR) model given as,

$$s_n = -\sum_{k=1}^{p} a_k s_{n-k} + G u_n, \tag{4.3}$$

where u_n is input with gain G, s_n output, and a_k are AR coefficients for model order p [39]. Equation 4.3 is termed autoregressive because the output s_n is regressed back upon itself. Taking the Z transform of Equation 4.3 allows a frequency domain interpretation of an AR model as an all pole transfer function $H(z)$

$$H(z) = \frac{G}{1 + \sum_{k=1}^{p} a_k z^{-k}}. \tag{4.4}$$

An AR model was implemented for feature extraction in the following way:

1. A 6^{th} order AR model is created for the unfiltered baseline run when no damage is present.
2. The baseline is estimated using the AR model and the prediction error calculated.
3. Unfiltered trial runs 1 to 18 are estimated using the baseline AR model and prediction error calculated.
4. The standard deviation of the prediction error for each run is calculated.

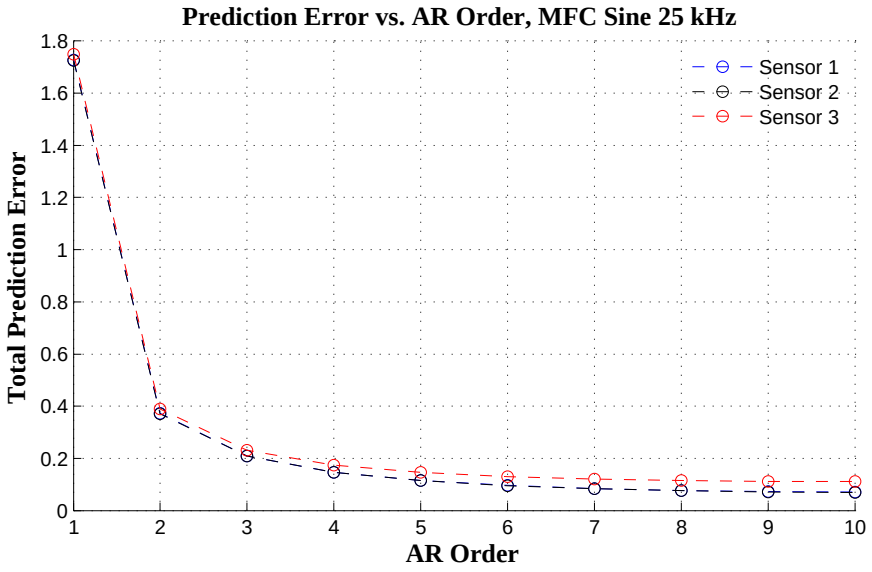

Figure 4.15: Standard deviation of AR prediction error

The order of the AR model was selected by increasing the model order until the total prediction error begin to reach an asymptotic value, Figure 4.15. Figure 4.16 is a plot of the standard deviation of prediction error verses crack length. Sensor 1 and 2 show an increasing trend with crack length while sensor 3 does not. These results are for the first 5000 points of the unfiltered time series data. When the analysis is performed over the entire length of the signal there is no discernable correlation with crack length. Additionally when the analysis is performed on bandpassed filtered data, no correlation exists between crack length.

Chapter 4, in part, is a reprint of the material as it appears in *Smart Structures and Materials & Nondestructive Evaluation and Health Monitoring*, Gregory J. Jarmer,

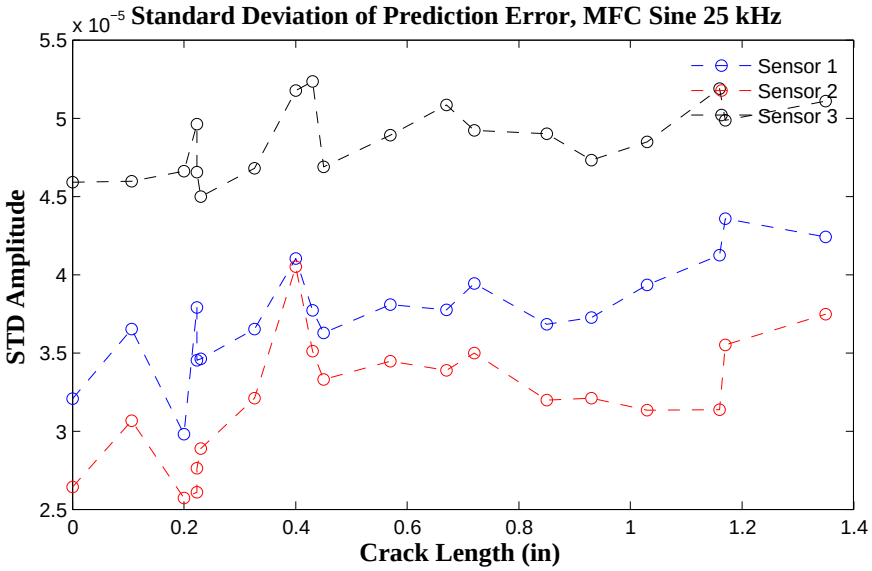

Figure 4.16: Standard deviation of AR prediction error

Michael D. Todd, 2009. The thesis author was the primary investigator and author of this paper.

Chapter 5

Conclusions

5.1 Introduction

Failure of a system due to damage is unwanted since it often results in loss of life and economic value. Currently, many systems are used past their designed life expectancy, in spite of age and damage accumulation, due to economic constraints. In response to this, tools are being developed to detect the formation of damage in both new and aging infrastructure. Structural Health Monitoring (SHM) is the process of implementing a damage detection strategy in near real time using periodic inspections of a system to determine the presence of damage. Inspection involves acquisition of the systems dynamic response, extraction of damage sensitive features from the response, and then classification of the extracted features to determine health status.

This thesis focused on the detection of fatigue cracks in metallic structures using guided ultrasonic waves (GUWs). An experiment was designed and conducted on test specimens in which fatigue cracks were grown through cyclic loading. Damage sensitive features were extracted from GUW time series using signal processing techniques based upon time domain, frequency domain, and modeling analysis.

5.2 Experimental Design Considerations

Experiments conducted in this thesis focused on inducing fatigue cracks in aluminum test specimens through cyclic loading. GUWs were induced with piezoelectric

based transducers. GUW measurements were taken at increments of approximately $0.075''$ of crack growth. Several issues need to be addressed in future experiments to validate results. The first issue is transducer bond conduction. Since the test is dynamic and the test specimen is placed in cyclic tension, the ability of the transducers to retain their original bond condition is a concern. The resulting change in a received signal due to a change in bond condition might be interpreted as a change due to damage. One method for possibly measuring the bond condition is to measure the electrical impedance of the transducer. This assumes that the impedance of a bonded transducer is determined by the bond condition and local mechanical impedance. As long as the local mechanical impedance does not change, a change in impedance is attributed to a change in bond condition.

The second issue is the effect of temperature variations on wave propagation and transducer characteristics. Just as a change in bond condition might be interpreted as a change due to damage, variations in temperate can be mistaken as damage. Possible compensation of temperature effects is through the training of a reference database for damage levels subject to known temperature changes.

5.3 Signal Processing Results

5.3.1 Time Domain Analysis

Damage sensitive features were extracted from GUW time series using signal processing techniques based upon time domain, frequency domain and modeling analysis. Modulated sine and chaotic sine waveforms were used as actuation signals at frequencies ranging from 25 to 100 kHz. Table 3.1 lists actuation and transducer pairs used during the experiment. Analysis was performed on sensor time series data that is normalized by a baseline signal condition.

Time domain analysis consisted of extracting features from the first arrival and entire waveform. Results for actuation signals and transducers are given in Tables 4.1 to 4.4. The labeling (1,2,3) corresponds to sensor 1, sensor 2 and sensor 3. The term : 2^{nd} means that the extracted feature is only able to detect change in the second half of the signal for crack lengths greater than 0.4 inches.

When the analysis is based upon the entire length of the waveform, the best

extracted feature is the standard deviation of the difference between the trail run and baseline. Additionally the chaotically modulated waveforms perform better than the sinusoidal waveforms.

When the first arrival is analyzed, the sinusoidal waveforms perform better than the chaotic waveforms. Every extracted feature except for the mean is able to detect the presence of damage. Of the three MFC sensors, 1 and 2 perform best. This is expected since sensors 1 and 2 are positioned down stream of the damage allowing the analysis of a waveform that is transmitted through the fatigue crack, Figure 3.6. In contrast sensor 3 is only able to detect damage due to reflections from crack formation. This when performing analysis based upon first arrival sensor 1 and 2 will have better performance.

Results for the piezoelectric disk are somewhat bias since transducers 1 and 2 became disbonded during testing preventing any data from being collected. Thus results are only shown for sensor 3.

5.3.2 Frequency Domain Analysis

Frequency domain analysis consists of transforming collected data from the time domain into the frequency domain using the discrete Fourier transform (DFT). Since the collected time series data is narrow band, extracted features in the frequency domain based upon amplitude will be similar to extracted features based upon amplitude in the time domain due to the linearity of the DFT. A change in peak values of the DFT for the first arrival waveform, Figure 4.13, was shown to correlate with crack growth.

5.3.3 Modeling Analysis

Autoregressive (AR) models were formed from baseline signals. The baseline models were used to predict waveforms collected from a damaged state. The standard deviation of the prediction error was correlated to crack length, Figure 4.16. Correlation to crack length was only successful when analysis was performed on the first arrival of the time series data. When the analysis is performed over the entire length of the signal there is no discernable correlation with crack length.

Taking the viewpoint that AR modeling is a process of spectrum matching that attempts to approximate a signals spectrum with an all pole model offers a possible explanation for why no correlation is shown with damage for analysis of the entire signal

length. Since the sensor data being fitted is relatively narrowband, fitting an AR model corresponds to fitting poles to a single peak in the frequency domain. Thus using prediction error or AR model coefficients as damage sensitive features will not be effective unless damage causes a change in a received signals spectrum, such as a shift in frequency or redistribution of the signals frequency content.

5.4 Future Work

Future work will consist of implementation of experiments that take into account environmental effects such as temperature and measurement of bond condition to assure that changes in a received signal are only due to damage. The sample spacing of induced waveforms should be reduced from current increments of $0.075''$ to $0.01''$ of crack growth to determine the minimum resolution of extracted features at detecting crack growth. Other types of induced waveforms, such as broadband and sinusoidal input at frequencies above 150 kHz, should be investigated to determine the effect of actuation frequency and bandwidth at detecting damage. Other signal processing techniques that employ methods to reduce unwanted effects from echos and dispersion need to be implemented to enhance the understanding of GUW wave interaction with damage. Additionally data-based modeling techniques, such as autoregressive moving average (ARMA) and state space embedding models, which take advantage of broadband input and chaotically-modulated probes will be investigated.

Bibliography

[1] National Transportation Safety Board (NTSB) Publications. Chalks ocean airways flight 101. *http://www.ntsb.gov/publictn/2007/AAR0704.htm*, 2009.

[2] National Transportation Safety Board (NTSB) Publications. Aloha airlines, flight 243. *http://www.ntsb.gov/publictn/1989/AAR8903.htm*, 2009.

[3] National Transportation Safety Board (NTSB) Publications. Natural gas distribution line break and subsequent explosion and fire. *http://www.ntsb.gov/publictn/2008/PAB0801.htm*, 2009.

[4] C.R. Farrar and K. Worden. An introduction to structural health monitoring. *Philosophical Transactions of the Royal Society A: Mathematical, Physical and Engineering Sciences*, 365(1851):303–315, 2007.

[5] Wieslaw J. Staszewski. *Advances in Smart Technologies in Structural Engineering*. Springer, 2003.

[6] Chuck Farrar. Se 207 fundamental of structural health monitoring lecture notes. Spring Term 2008.

[7] D. Pines and A.E. Aktan. Status of structural health monitoring of long-span bridges in the United States. *Progress in Structural Engineering and materials*, 4(4), 2002.

[8] C. Boller. Ways and options for aircraft structural health management. *Smart materials and structures*, 10(3):432–440, 2001.

[9] C. Brand, C. Boller, and D.C.A.A.G. MUNCHEN. Identification of Life Cycle Cost Reductions in Structures With Self-Diagnostic Devices, 2000.

[10] Nasa dc-9 research airplane. *www.nasa.gov*.

[11] Lockheed martin f-16 fighting falcon. *http://www.lockheedmartin.com/products/f16/*.

[12] AE Aktan, FN Catbas, KA Grimmelsman, and CJ Tsikos. Issues in infrastructure health monitoring for management. *Journal of Engineering Mechanics*, 126(7):711–724, 2000.

[13] C.R. Farrar. Vibration-based structural damage identification. *Philosophical Transactions of the Royal Society A: Mathematical, Physical and Engineering Sciences*, 359(1778):131–149, 2001.

[14] Peter E. Hart Richard O. Duda and David G. Stork. *Pattern Classification*. John Wiley and Sons, second edition, 2001.

[15] Victor Giurgiutiu. Tuned Lamb Wave Excitation and Detection with Piezoelectric Wafer Active Sensors for Structural Health Monitoring. *Journal of Intelligent Material Systems and Structures*, 16(4):291–305, 2005.

[16] H. Kolsky. *Stress Waves in Solids*. Dover Publications, 1963.

[17] Joseph L. Rose. *Ultrasonic Waves in Solid Media*. Cambridge University Press, 1999.

[18] G. F. Roach. *Wave Scattering by Time-Dependent Pertubations*. Prinction University Press, 2007.

[19] WJ Staszewski. Advanced data pre-processing for damage identification based on pattern recognition. *International Journal of Systems Science*, 31(11):1381–1396, 2000.

[20] C. Biemans, WJ Staszewski, C. Boller, and GR Tomlinson. Crack detection in metallic structures using broadband excitation of acousto-ultrasonics. *Journal of Intelligent Material Systems and Structures*, 12(8):589, 2001.

[21] WH Leong, WJ Staszewski, BC Lee, and F. Scarpa. Structural health monitoring using scanning laser vibrometry: III. Lamb waves for fatigue crack detection. *Smart Materials and Structures*, 14(6):1387, 2005.

[22] M. Ryles, F.H. Ngau, I. Mcdonald, and W.J. Staszewski. Comparative study of nonlinear acoustic and Lamb wave techniques for fatigue crack detection in metallic structures. *Fatigue & Fracture of Engineering Materials & Structures*, 31(8 Fatigue Crack Detection Using Smart Sensor Technologies-Guest Editor: Wieslaw J. Staszewski):674–683, 2008.

[23] V. Giurgiutiu. Lamb wave generation with piezoelectric wafer active sensors for structural health monitoring. *Smart Structures and Materials 2003*, 5056:111–122, 2003.

[24] D.N. Alleyne and P. Cawley. The interaction of lamb waves with defects. *IEEE Transactions on Ultrasonics, Ferroelectrics and Frequency Control*, 39(3):381–397, May 1992.

[25] A. Raghavan and C.E.S. Cesnik. Guided-wave signal processing using chirplet matching pursuits and mode correlation for structural health monitoring. *Smart Materials and Structures*, 16(2):355, 2007.

[26] A.V. Oppenheim and R. W. Schafer. *Discrete Time Signal Processing*. Prentice Hall Publishers, 1998.

[27] Jeong-Beom Ihn and Fu-Kuo Chang. Detection and monitoring of hidden fatigue crack growth using a built-in piezoelectric sensor/actuator network: I. diagnostics. *Smart Materials and Structures*, 13(3):609–620, 2004.

[28] M. Niethammer, L.J. Jacobs, J. Qu, and J. Jarzynski. Time-frequency representations of Lamb waves. *The Journal of the Acoustical Society of America*, 109:1841, 2001.

[29] BC Lee and WJ Staszewski. Modelling of Lamb waves for damage detection in metallic structures: Part II. Wave interactions with damage. *Smart Materials and Structures*, 12(5):815–824, 2003.

[30] Y. Cho, DD Hongerholt, and JL Rose. Lamb wave scattering analysis for reflector characterization. *IEEE Transactions on Ultrasonics, Ferroelectrics and Frequency Control*, 44(1):44–52, 1997.

[31] SW Liu, SK Datta, and TH Ju. Transient scattering of Rayleigh-Lamb waves by a surface-breaking crack: comparison of numerical simulation and experiment. *Journal of Nondestructive Evaluation*, 10(3):111–126, 1991.

[32] Lennart Ljung. *System Identification Theory for the User*. Prentice Hall Publishers, 1987.

[33] A.C. Cobb, J.E. Michaels, and T.E. Michaels. Experimental verification of a Kalman filter approach for estimating the size of fastener hole fatigue cracks. In *Health Monitoring of Structural and Biological Systems 2008. Edited by Kundu, Tribikram. Proceedings of the SPIE*, volume 6935, pages 69350Y–69350Y, 2008.

[34] H. Sohn, J.A. Czarnecki, and C.R. Farrar. Structural health monitoring using statistical process control. *Journal of Structural Engineering*, 126:1356, 2000.

[35] Joseph L. Rose. A baseline and vision of ultrasonic guided wave inspection potential. *Journal of Pressure Vessel Technology*, 124(3):273–282, 2002.

[36] Geof Tomlinson Wieslaw Staszewski, Christian Boller. *Health Monitoring of Aerospace Structures*. Wiley, 2004.

[37] P.C. Paris. *The Stress Analysis of Cracks Handbook*. Hall Publishers, 1990.

[38] T.L. Anderson. *Fracture Mechanics, Fundamentals and Applications*. CRC Press, third edition, 2005.

[39] J. Makhoul. Linear prediction: A tutorial review. *Proceedings of the IEEE*, 63(4):561–580, April 1975.

[40] E. ASTM. 647,standard test method for measurement of fatigue crack growth rates. *Annual book of ASTM standards*, 3:647–90, 1994.

[41] Julius S. Bendat and Allan G. Piersol. *Random Data Analysis and Measurement Procedures*. John Wiley and Sons, third edition, 2000.

[42] Frank Bruni. Head scratchers: the hen egg.

[43] T.R. Fasel, H. Sohn, and C.R. Farrar. Application of Frequency Domain ARX Models and Extreme Value Statistics to Damage Detection. In *Smart Structures and Materials 2003: Smart Systems and Nondestructive Evaluation for Civil Infrastructures. Edited by Liu, Shih-Chi. Proceedings of the SPIE*, volume 5057, pages 145–156, 2003.

[44] Timothy R. Fasel, Michael D. Todd, and Gyuhae Park. Active chaotic excitation for bolted joint monitoring. In Masayoshi Tomizuka, Chung-Bang Yun, and Victor Giurgiutiu, editors, *Smart Structures and Materials 2006: Sensors and Smart Structures Technologies for Civil, Mechanical, and Aerospace Systems*, volume 6174, page 61741S. SPIE, 2006.

[45] V. Giurgiutiu and A. Cuc. Embedded non-destructive evaluation for structural health monitoring, damage detection, and failure prevention. *The Shock and Vibration Digest*, 37(2):83, 2005.

[46] JE Gubernatis, E. Domany, and JA Krumhansl. Formal aspects of the theory of the scattering of ultrasound by flaws in elastic materials. *Journal of Applied Physics*, 48:2804, 1977.

[47] JE Gubernatis, E. Domany, JA Krumhansl, and M. Huberman. The Born approximation in the theory of the scattering of elastic waves by flaws. *Journal of Applied Physics*, 48:2812, 1977.

[48] S. Gupta, A. Ray, and E. Keller. Symbolic time series analysis of ultrasonic data for early detection of fatigue damage. *Mechanical Systems and Signal Processing*, 21(2):866–884, 2007.

[49] Simon Haykin. *Adaptive Filter Theory*. Prentice Hall Publishers, third edition, 1996.

[50] R.K. Ing and M. Fink. Time-Reversed Lamb Waves. *ieee transactions on ultrasonics, ferroelectrics, and frequency control*, 45(4), 1998.

[51] Steven M. Kay. *Fundamentals of Statistical Signal Processing Detection Theory*. Prentice Hall Publishers, 1998.

[52] Francesco Lanza Discalea, Howard Matt, Ivan Bartoli, Stefano Coccia, Gyuhae Park, and Charles Farrar. Health Monitoring of UAV Wing Skin-to-spar Joints using Guided Waves and Macro Fiber Composite Transducers. *Journal of Intelligent Material Systems and Structures*, 18(4):373–388, 2007.

[53] Y. Lei, AS Kiremidjian, KK Nair, JP Lynch, KH Law, TW Kenny, E. Carryer, and A. Kottapalli. Statistical damage detection using time series analysis on a structural health monitoring benchmark problem. In *Proceedings of 9 th International Congress on Applications of Statistical and Probability in Civil Engineering*, 2003.

[54] Michel Goossens Frank Mittelbach and Alexander Samarin. *The LATEX Companion*. Addison-Wesley, 1994.

[55] Henry W. Ott. *Noise Reduction Techniques in Electronic Systems*. John Wiley and Sons, 1988.

[56] YH Pao and CC Chao. Diffractions of flexural waves by a cavity in an elastic plate. *AIAA J*, 2(11):2004–2010, 1964.

[57] Athanasios Papoulis. *Probability, Random Variables, and Stochastic Processes*. McGraw Hill, 1984.

[58] H. Sohn, C.R. Farrar, N.F. Hunter, and K. Worden. Structural health monitoring using statistical pattern recognition techniques. *Transactions-American Society of Mechanical Engineers Journal of Dynamic Systems Measurement And Control*, 123(4):706–711, 2001.

[59] Peter J. Shull, editor. *Nondestructive Evaluation*. Marcel Dekker, 2002.